

MATERIALS SCIENCE

From oxide epitaxy to freestanding membranes: Opportunities and challenges

SooHo Choo^{1†}, Shivashesh Varshney^{1†}, Huan Liu², Shivam Sharma², Richard D. James², Bharat Jalan^{1*}

Motivated by the growing demand to integrate functional oxides with dissimilar materials, numerous studies have been undertaken to detach a functional oxide film from its original substrate, effectively forming a membrane, which can then be affixed to the desired host material. This review article is centered on the synthesis of functional oxide membranes, encompassing various approaches to their synthesis, exfoliation, and transfer techniques. First, we explore the characteristics of thin-film growth techniques with emphasis on molecular beam epitaxy. We then examine the fundamental principles and pivotal factors underlying three key approaches of creating membranes: (i) chemical lift-off, (ii) the two-dimensional layer-assisted lift-off, and (iii) spalling. We review the methods of exfoliation and transfer for each approach. Last, we provide an outlook into the future of oxide membranes, highlighting their applications and emerging properties.

INTRODUCTION

There is an increasing interest in integrating functional oxides with semiconductor or quantum information devices. This is encouraged by the demands of vertical integration or back-end-of-the-line (BEOL) integration, the major stage in semiconductor manufacturing where different functional layers are interconnected. This need underscores the importance of atomically precise synthesis techniques for layers that serve as metal electrodes, dielectrics, or functionalized channel materials on the selected wafer (Fig. 1A). Integrating optimal materials for each layer poses synthesis obstacles, most often involving crystal quality and interfacial defects that may compromise the overall electrical properties of the device.

Epitaxial growth of three-dimensional (3D) functional oxide films is typically achieved on compatible wafers with similar crystal symmetry and lattice parameters. However, this requirement of epitaxial growth—relying on lattice/symmetry matching—limits the integration of diverse material systems and their application in devices. For instance, thin-film devices often exhibit lattice mismatches between layers, as illustrated in Fig. 1B for perovskite oxides. This issue becomes even more pronounced when combining dissimilar materials, such as oxides and conventional semiconductors, leading to high densities of misfit dislocations, threading dislocations, anti-phase boundaries (APBs), and stacking faults, as illustrated in Fig. 1C. Additionally, atomic layer nucleation differences between oxide A over oxide B and vice versa can complicate the growth of sharp interfaces in oxide B/oxide A/oxide B heterostructures. These epitaxial growth challenges can degrade device performance by causing interfacial charge trapping, high leakage, and slow switching speeds.

Freestanding oxide films offer a way to overcome the epitaxial constraints of substrates. These membranes, which can bend, fold, or stretch, are capable of mechanical deformation, enabling functionalities not achievable in constrained or unstressed films of the same composition (1–5). Membranes can be transferred onto chemically and

structurally incompatible wafers, leading to the formation of artificial heterostructures, including 3D-over-3D structures (i.e., bicrystals), 3D-over-two-dimensional (2D) structures, or virtual substrates (6–14), as illustrated in Fig. 1D. In 3D-3D materials, dangling bonds and a flexible lattice provide more degrees of freedom than in 2D materials, allowing for bond cleavage or reformation, which in turn may enable charge transfer and orbital/spin interactions. The interplay of multiple degrees of freedom—such as charge, orbital, spin, and lattice—exhibited by complex oxides can result in intriguing quantum functionalities (15, 16). These membranes can be uniformly strained to achieve states unattainable in bulk crystals, or they can be controllably rippled, wrinkled, or bubbled to create strain gradients (17–23).

An exciting direction involves devices created by stacking and twisting oxide membranes at different in-plane rotation angles, known as Moirétronics, stacktronics, or twistronics. This emerging field allows for the tuning of fundamental properties such as ferroelectricity, chirality, and superconductivity (24–26). A particularly compelling opportunity arises from precisely stacking atomically smooth interfaces to form 3D/3D lattices. These stacks can break various symmetries, create chirality, and introduce interlayer coupling, potentially giving rise to quantum states not found in the parent compounds (27–30). Atomically thin freestanding films of functional oxides also enable the study of individual point defects and complex periodic or quasiperiodic defect arrays. Mechanical deformations in clamped-free membranes can lead to origami-inspired structures (31), which are gaining traction in various technologies.

In this review, we highlight recently developed methods for creating oxide membranes, focusing on their growth and exfoliation/transfer techniques. First, we discuss thin-film growth methods for oxide thin films, including magnetron sputtering, pulsed laser deposition (PLD), and molecular beam epitaxy (MBE), with particular emphasis on hybrid MBE. Next, we examine three representative membrane creation techniques—chemical lift-off, 2D layer-assisted lift-off, and mechanical lift-off—analyzing their advantages and disadvantages in relation to the different thin-film growth methods. Last, we provide an outlook on the potential applications of functional oxide membranes in devices and their importance for advancing fundamental physics research. The ability to produce large-area, high-quality, and precisely

¹Department of Chemical Engineering and Materials Science, University of Minnesota, Minneapolis, MN 55455, USA. ²Department of Aerospace Engineering and Mechanics, University of Minnesota, Minneapolis, MN 55455, USA.

*Corresponding author. Email: bjalan@umn.edu
†These authors contributed equally to this work.

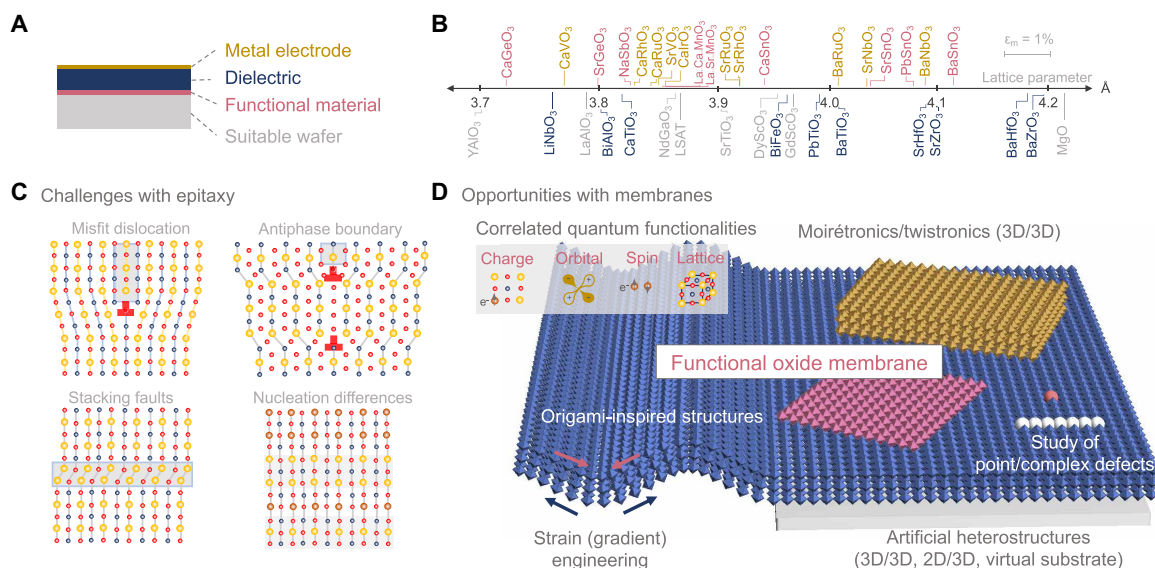


Fig. 1. Challenges with thin-film epitaxy and opportunities with thin-film membranes. (A) A schematic representing a device structure, showing the key layers required for device performance. A metal electrode is shown in gold, the Dielectric/Ferroelectric material is shown in blue, functional material/semiconductor is shown in pink, and a suitable wafer is shown in gray. (B) Lattice parameter number line of perovskite oxides that can be used as a metal electrode, dielectric/ferroelectric, functional material, and suitable wafer, illustrating many near epitaxial relationships possible in these oxides. (C) Challenges for epitaxial growth of each of the device layers. Interfacial defects such as misfit dislocations, antiphase boundaries, stacking faults, and nucleation differences of one layer over another. (D) A representative free-standing membrane offers opportunities in 3D/3D tristronics/Moiré/tristronics/stacktronics, addressing several limitations of thin films. Here, 3D refers to materials with dangling bonds.

aligned functional oxide membranes is key to further progress in this field, enabling breakthrough advancements.

THIN-FILM MEMBRANE GROWTH METHODS

High crystalline quality and reproducibility are essential when choosing a growth method, ideally providing atomic-scale control for the precise synthesis of single crystals. Versatility is also important, enabling the growth of diverse material systems and smooth transitions between them. The method should produce sharp interfaces to facilitate the study of interfacial phenomena and be modular for easy system upgrades. These goals are met by three main thin-film growth techniques for functional oxides: magnetron sputtering, PLD, and MBE. This review focuses primarily on MBE for membrane synthesis.

MAGNETRON SPUTTERING

As shown in Fig. 2A, magnetron sputtering occurs in a high vacuum chamber, where sintered targets are used to achieve the desired oxide composition. Magnetron sputtering is a physical vapor deposition technique used to deposit thin films onto substrates. In this process, a high-vacuum chamber houses a target material that is negatively biased. A gas, such as argon, is ionized to create a plasma, which bombards the target with positively charged ions. This impact causes atoms from the target to sputter and travel across the chamber to deposit onto a heated substrate. A magnetic field generated by the magnet enhances plasma density and stability, leading to uniform and high-quality film deposition. However, the use of high-energy charged ions may promote the introduction of point defects into the film as it grows. Owing to this, the defect/dislocation density

obtained in films is generally higher than the other two approaches, PLD and MBE (32). At present, there have been limited studies on membranes using this approach (33).

PULSED LASER DEPOSITION

PLD has been a popular technique for membrane and heterostructure synthesis of complex oxides with atomic level control over structure. In this approach, a high-power pulsed laser (34, 35) is directed onto a target material inside a vacuum chamber as illustrated in Fig. 2B. The laser pulse vaporizes the target, generating a plasma plume that consists of various energetic species, including atoms, ions, molecules, and particulates. This vaporized material is then deposited as a thin film onto a substrate, which is typically placed facing the target. Typically, a KrF excimer laser (wavelength: 248 nm) is used, but the laser source can be changed. PLD for oxide synthesis often employs high oxygen background pressure to ensure complete oxygenation of oxide films, but it also lowers the kinetic energies of ablating species (35).

Although the basic setup of PLD is relatively straightforward, the underlying physical growth processes are quite intricate. This method has been widely used in membrane synthesis using a sacrificial layer (2, 20, 23, 26, 28, 35–61) or a 2D material-assisted approach (62, 63–72), and is discussed later in this paper.

MOLECULAR BEAM EPITAXY

MBE is a thin-film growth technique that operates in an ultrahigh vacuum environment with base pressures typically in the range of 10^{-8} to 10^{-10} torr. It utilizes molecular beams from high-purity elemental sources to grow epitaxial films. The system is maintained at

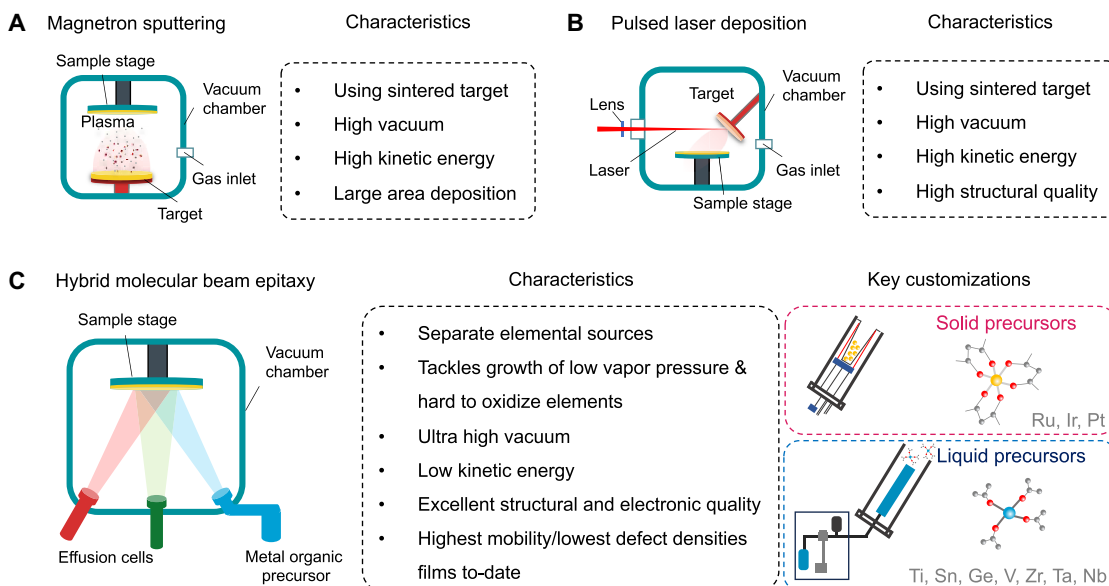


Fig. 2. Schematic representation of epitaxial thin-film growth methods and their key characteristics. (A) A magnetron sputtering system. The sputter of a target material results in epitaxial growth on the heated substrate. (B) PLD system. A laser located outside the system is incident on the target, which creates a plume resulting in epitaxial growth on the heated substrate. (C) MBE system. Pure elemental sources are used to grow epitaxial films on a heated substrate. The hybrid MBE system uses metal-organic solid and liquid precursors addressing the issues of low vapor pressure and hard to oxidize elements. The representative solid and liquid precursors are shown in pink and blue box respectively.

such low pressures by using turbomolecular pumps, helium-cooled cryogenic pumps, liquid nitrogen-cooled shrouds (to minimize surface outgassing), and high-temperature baking. This ensures minimal impurity incorporation into the film (73). The mean free path of the sublimated or evaporated species exceeds the distance between the source and substrate, preventing collisions between the growth species before they reach the substrate. MBE systems feature shutters for rapid switching between sources, enabling the growth of high-quality heterostructures. In situ monitoring tools like quartz crystal monitors (QCMs), beam flux monitors (BFMs), and reflection high-energy electron diffraction (RHEED) provide additional control and precision during growth.

To accurately control the stoichiometry of cations in the film, an adsorption-controlled growth of the film is desired. A “growth window” has been demonstrated in a number of oxide films grown by MBE. Within this window, the film self-regulates its stoichiometry. This was first achieved for GaAs and later for complex oxides using MBE (74, 75). The growth window of oxides is often found only at high temperatures or at ultralow pressure. For example, growing SrTiO₃ using conventional MBE within the thermodynamic growth window is not feasible due to the inaccessible growth conditions requiring low gas pressure of SrO and high substrate temperatures (76). Without a feasible growth window, the stoichiometry of SrTiO₃ is limited by the degree of flux control. For example, a 0.1% drop in Sr flux corresponds to about $2 \times 10^{19} \text{ cm}^{-3}$ vacancy concentration (77). The development of hybrid MBE overcame this issue by replacing elemental Ti by the liquid precursor titanium tetraisopropoxide (TTIP), as shown in Fig. 2C (76). The utilization of this volatile metal-organic precursor led to a large MBE growth window (76) and also helped to achieve a greatly increased growth rate exceeding 600 nm/hour (78). It has recently been demonstrated that the hybrid MBE growth window can also exist by co-supplying TTIP and Sr,

without supplying additional oxygen (79). A record-high electron mobility exceeding $32,000 \text{ cm}^2 \text{ V}^{-1} \text{ s}^{-1}$ (at 1.8 K) was found in hybrid MBE-grown La-doped SrTiO₃ on SrTiO₃ (001) substrate (80), higher than that of bulk single crystals (81). The mobility exceeded $128,000 \text{ cm}^2 \text{ V}^{-1} \text{ s}^{-1}$ (at 1.8 K) when strained in hybrid MBE-grown La-doped SrTiO₃ on LSAT (001) substrate (82). Similarly, low-temperature dielectric constant exceeded that of bulk single crystal in hybrid MBE-grown SrTiO₃ films (83). Hybrid MBE has been successfully used to grow single-crystalline films of various titanates, including BaTiO₃ (84, 85), CaTiO₃ (86), and GdTiO₃ (87), as well as stannates like BaSnO₃ (88), SrSnO₃ (89), and CaSnO₃ (90). It has also been applied to vanadates such as LaVO₃ (91), (La,Sr)VO₃ (92), and several others (93–96).

The hybrid MBE technique has been further expanded by incorporating solid metal-organic precursors that can be directly loaded into an effusion cell and sublimated, producing molecular beams of metal precursors that are typically hard to evaporate, such as platinum (Pt), iridium (Ir), and ruthenium (Ru) (97). These metals are also challenging to oxidize. Solid precursors like platinum(II) acetylacetonate [Pt(acac)₂], iridium(III) acetylacetonate [Ir(acac)₃], and ruthenium(III) acetylacetonate [Ru(acac)₃], which consist of metal atoms bonded to oxygen, have been utilized to grow phase-pure, single-crystalline Pt films as well as binary oxides such as IrO₂ (98) and RuO₂ (99). Additionally, complex oxides like SrIrO₃ (100), SrRuO₃ (101), and Sr₂RuO₄ (102), and metallic films of Ir and Ru were successfully grown with the solid precursors (103). A key advantage of these solid precursors is that they eliminate the need for a gas inlet system typically required to supply liquid precursors from outside the MBE system. The ideal precursors for this process should be air stable and have low vapor pressures ($\sim 10^{-10}$ torr) at room temperature, but with vapor pressures in the range of 10^{-5} torr at effusion cell temperatures of a few hundred degrees (100° to 200°C).

The successful use of volatile metal-organic precursors in hybrid MBE has also influenced the PLD community, leading to their adoption for growing complex oxides. This approach, known as hybrid PLD (HPLD), has enabled adsorption-controlled growth, exemplified by the successful deposition of SrTiO₃ films using HPLD (32). More recently, it has also been used to grow KTaO₃ films (104).

MEMBRANE SYNTHESIS APPROACHES

There is a substantial progress in measures taken to separate the grown epitaxial oxide thin film from its substrate. For instance, the growth substrate can be removed by using an etchant or by laser (105, 106). However, the cost of the substrate for most oxide materials is high, and the use of lasers or harsh etchants can potentially

damage the film. Several other methods have been suggested to decouple the films from the substrate (Fig. 3A), such as chemical lift-off (sacrificial layer method), 2D layer-assisted lift-off (remote and vdW epitaxy), and mechanical lift-off (spalling). Moreover, these methods must also be compatible with the thin-film growth technique. For instance, approaches to create functional membranes may require different growth techniques such as PLD over MBE due to the choice of lift-off layer. The concepts, characteristics, and techniques suitable for membrane growth and release are discussed below.

CHEMICAL LIFT-OFF

As early as 1980s, chemical methods were developed to make free-standing films (107, 108). Chemical lift-off involves sacrificing a layer

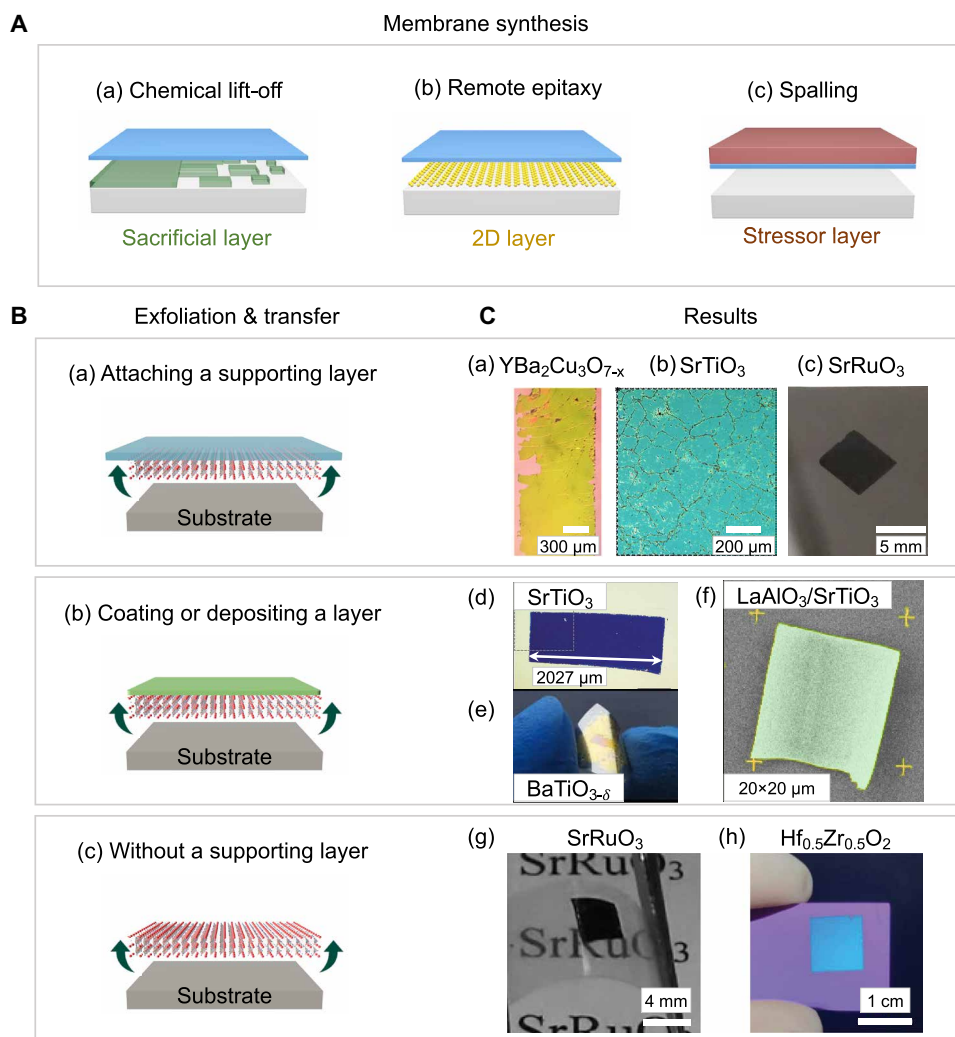


Fig. 3. Schematic representation of the membrane synthesis methods. (A) Representative ways to synthesize thin-film membranes. (B) Representative ways to exfoliate and transfer the grown thin-film membrane: (a) by attaching a polymer supporting layer, (b) by coating a polymer layer or depositing a metal layer, and (c) by detaching the grown film without any support. (C) Representative membranes produced using each of the exfoliation and transfer methods. (a) Free-standing YBa₂Cu₃O_{7-x} membranes on a polypropylene carbonate (PPC)/PDMS supporting layer. (b) Free-standing SrTiO₃ on a Si substrate by attaching the screen protector (silicon-coated PET). Reproduced with permission from the American Chemical Society (4). (c) Free-standing SrRuO₃ by attaching thermal release tape and coating PMMA. (d) SrTiO₃ produced by coating a cellulose acetate butyrate (CAB) layer transferred on TiN/Si. (e) BaTiO_{3-δ} produced by depositing Ni layer using remote epitaxy on Au/Cr/Pt. (f) Scanning electron microscopy image for spalling results of LaAlO₃/SrTiO₃. (g) SrRuO₃ membrane produced by scooping directly on PET. (h) Hf_{0.5}Zr_{0.5}O₂ membrane produced by scooping the membrane on SiO₂/Si. All images reproduced with permission from respective publishers (4, 42, 65, 109, 179).

between the substrate and the film as shown in Fig. 3A (a). The grown film is detached from the substrate by dissolving/etching the sacrificial layer (38, 109). It is important that the sacrificial layer satisfies some common criteria, as listed in (110), of (i) compatibility between the sacrificial layer and the film (epitaxial growth of film should be possible on the sacrificial layer), (ii) selectivity (such that etching the sacrificial layer does not damage the film and the released substrate is reusable; it is conceivable that longer etching time can cause unintended damage to the film), (iii) stability [the sacrificial layer should be stable at high growth temperatures (typically 800°C); this thermodynamic stability is essential to grow the film without any intermixing or formation of unintended phases], (iv) processibility (the layer should be grown inside the growth chamber with atomic layer control and precision), and (v) tunability (the lattice parameter of the layer should be tunable to match that of the film).

The type of sacrificial layer should be carefully selected depending on functional oxide film. $\text{Sr}_3\text{Al}_2\text{O}_6$, alloyed with $\text{Ca}_3\text{Al}_2\text{O}_6$ and $\text{Ba}_3\text{Al}_2\text{O}_6$, which can be dissolved in water, has been the most widely adopted sacrificial layers for perovskite oxides (58, 109, 111). The higher the electronegativity of the alkaline earth metal used ($\text{Ca}^{2+} > \text{Sr}^{2+} > \text{Ba}^{2+}$), the more difficult it is to dissolve in water (112, 113). While Ba substitution makes for easy hydrolysis, it also causes macroscopic distortions in the lattice of the functional oxide film, as discussed later in this section. More recently, tetragonal-phase $\text{Sr}_4\text{Al}_2\text{O}_7$, a member of the $(\text{Ca}, \text{Sr}, \text{Ba})_4\text{Al}_2\text{O}_7$ family, was introduced (114, 115) as a sacrificial layer material. The Al-O network is more discrete, and the concentration of SrO is higher, in $\text{Sr}_4\text{Al}_2\text{O}_7$ compared to $\text{Sr}_3\text{Al}_2\text{O}_6$, resulting in increased water solubility and thus shorter dissolving time. Other widely used sacrificial layers are $\text{La}_{0.7}\text{Sr}_{0.3}\text{MnO}_3$ (etched in acidic solution of KI + HCl) (38), SrRuO_3 (etched in NaIO_4 solution) (116), SrVO_3 (etched in water) (117), $\text{YBa}_2\text{Cu}_3\text{O}_7$ (etched in HCl) (59), and $\text{SrCoO}_{2.5}$ (etched in vinegar) (118). The lattice parameters of these sacrificial layers are similar to many perovskite oxides (3.8 to 4.1 Å). This class of complex sacrificial layers has successfully produced free-standing films of a diverse material systems such as SrTiO_3 (109, 119, 120), BaTiO_3 (2, 3, 46, 121), $\text{YBa}_2\text{Cu}_3\text{O}_{7-x}$ (59), BiFeO_3 (4, 120), SrRuO_3 (56, 122, 123), $\text{La}_{0.7}\text{Ca}_{0.3}\text{MnO}_3$ (111), $\text{La}_{0.7}\text{Sr}_{0.3}\text{MnO}_3$ (54), and superlattices, to name a few.

In the realm of thin-film growth techniques, PLD is particularly advantageous for the sacrificial layer method, primarily due to the ease with which $\text{Sr}_3\text{Al}_2\text{O}_6$ can be grown using this technique. Since the first report on the use of a $\text{Sr}_3\text{Al}_2\text{O}_6$ sacrificial layer, most research on free-standing oxide membranes was conducted using PLD. To our knowledge, there is no report on the use of sputtering alone to grow the sacrificial layer. Instead, $\text{PbTiO}_3/\text{SrTiO}_3$ superlattices were grown on a $\text{Sr}_3\text{Al}_2\text{O}_6$ sacrificial layer by sputtering after the $\text{Sr}_3\text{Al}_2\text{O}_6$ sacrificial layer was deposited by PLD (124). Similarly, a $\text{Sr}_3\text{Al}_2\text{O}_6$ sacrificial layer capped by a SrTiO_3 layer was grown on a SrTiO_3 substrate using PLD; then, an La-doped SrTiO_3 film was grown by MBE by ex situ transferring of $\text{SrTiO}_3/\text{Sr}_3\text{Al}_2\text{O}_6/\text{SrTiO}_3$ from a PLD to an MBE chamber (125). Although various free-standing membranes, such as SrTiO_3 , BaFeO_3 , PbTiO_3 , and BaTiO_3 , were produced solely by MBE (21, 120, 126–128) using an $\text{Sr}_3\text{Al}_2\text{O}_6$ sacrificial layer, the growth of such complex sacrificial layers is not straightforward owing to the complexity of MBE growth for $\text{Sr}_3\text{Al}_2\text{O}_6$.

Producing free-standing membranes with MBE using a complex sacrificial layer is like trying to make a soufflé with one hand tied behind your back—doable, but only if you are a culinary wizard. This is evident by the fact that as of 2023, only $1/10$ of all publications used

MBE alone to grow membranes. The challenge of MBE growth of free-standing membranes is effectively circumvented by the use of binary alkaline earth oxide sacrificial layers (110). These alkaline earth oxide sacrificial layers are easier to grow in MBE because alkaline earth metals can be sublimated at a low effusion cell temperature of 300° to 500°C and they readily oxidize in molecular oxygen to form corresponding oxides. The binary oxide sacrificial layer system (Mg, Ca, Sr, Ba)O can be alloyed to achieve extensive tuning of lattice parameters. When combined with complex sacrificial layers, they allow continuous tuning of lattice parameter from 2.98 to 5.12 Å, a range unreachable with the current commercially available substrates (110). Binary oxides with a rock salt structure will grow on the perovskite substrate with an in-plane rotation of 45°. These oxides can then be used as a template to grow perovskite structures. Epitaxial layer-by-layer and step-flow growth of SrTiO_3 has been shown on 2- to 60-nm-thick SrO sacrificial layer using hybrid MBE on LAO (001) and LSAT (001) substrates, respectively (110). Epitaxial growth of a $\text{SrTiO}_3/\text{BaSnO}_3$ heterostructure on a BaO sacrificial layer and a $\text{SrTiO}_3/\text{CaSnO}_3$ heterostructure on a $\text{Ba}_{1-x}\text{Ca}_x\text{O}$ sacrificial layer has also been demonstrated using hybrid MBE (110). There has also been some success in PLD on the use of a BaO sacrificial layer to grow $\text{SrTiO}_3/\text{BaTiO}_3$ heterostructures (129) and CrN membranes (36), demonstrating their versatility in membrane synthesis.

Generally, full width at half maximum (FWHM) of the rocking curve around the (002) diffraction condition is used to determine the crystallinity of a (001)-oriented thin film. However, it was found that the binary oxides were hygroscopic: Samples reacted with moisture in air, leading to macroscopic distortions, changing the FWHM of the film. An FWHM of 10 nm in a SrTiO_3 film was found to be $\sim 0.14^\circ$ grown on 2-nm SrO on LSAT substrate (110). The FWHM increased to twice this value when sample was not capped with amorphous Si capping layer. Therefore, future efforts should perform in situ diffraction studies to accurately determine the FWHM of SrTiO_3 on a binary oxide sacrificial layer. The practice of transferring and exfoliating the sample in a glove box can be adopted to preserve the macroscopic features.

The hygroscopic nature of the binary oxide sacrificial layers such as SrO and BaO substantially enhanced the dissolution time to a few minutes (<5 min) in water, according to the following reaction: $\text{SrO} + \text{H}_2\text{O} \rightarrow \text{Sr}(\text{OH})_2$. This is important for films that are sensitive to long exposure in water when using a $\text{Sr}_3\text{Al}_2\text{O}_6$ sacrificial layer. For instance, the nickelate series commonly sought after for their superconducting properties and other intriguing phenomena can be potentially damaged in long exposure to water. A fast, soluble, and easy to synthesize sacrificial layer is therefore needed by the membrane community.

While binary oxides have proven to be extremely useful for membrane synthesis in MBE, there are other ways to use complex sacrificial layers in MBE. Hybrid MBE may offer solutions for the growth of complex sacrificial layers like $\text{Sr}_3\text{Al}_2\text{O}_6$ by carefully selecting a precursor to supply aluminum, such as dimethylaluminum isopropoxide (DMAI). This idea was previously explored using atomic layer deposition (ALD) (130). For example, a sacrificial layer of SrRuO_3 can be grown in hybrid MBE where Ru is supplied using $\text{Ru}(\text{acac})_3$ precursor (97, 101) and of SrVO_3 which can be grown by supplying V using a vanadium oxitriisopropoxide (VTIP) precursor (95). Similar precursors can be selected to grow other complex sacrificial layers (131–136); however, their use as a sacrificial layer in hybrid MBE remains to be explored.

Another approach is to use a sacrificial layer of $\text{Sr}_3\text{Al}_2\text{O}_6$, prepared *ex situ* in a chemical solution. For example, this sacrificial layer can be prepared by the metal nitrate precursor solution method, followed by high temperature thermal treatment (112). The sacrificial layer has been shown to crystallize in vacuum annealing and then used to grow functional oxides of $\text{La}_{0.7}\text{Sr}_{0.3}\text{MnO}_3$ in PLD (113). The hybrid MBE growth of an epitaxial, single-crystalline SrTiO_3 film on this sacrificial layer was recently demonstrated (137).

To summarize, the main advantages of using the sacrificial layer method are that (i) it allows single-crystalline growth of functional oxides, (ii) it produces large-area membranes, (iii) it promotes substrate reuse, and (iv) it can be readily adopted with growth techniques like MBE, hybrid MBE, or PLD. The cornerstone challenge is handling the exfoliated membrane so as to carefully transfer it to a desired host substrate without damage. Strategies for overcoming this challenge in the transfer processes are discussed in the “Membrane Exfoliation and Transfer Processes” section.

2D LAYER-ASSISTED LIFT-OFF

The marriage of 2D materials as sacrificial materials with 3D functional films is fascinating (138). Such 2D interlayers can break the strong bond that exists between the film and the substrate (17). Films grown on top of 2D materials have weak out-of-plane van der Waals (vdW) bonds that typically allow the grown film to separate from the substrate, as shown in Fig. 3A (b) (139). Typical 2D materials include graphene (65), transition metal dichalcogenides (TMDCs) (140), and h-BN (141). Among these, graphene is the most widely used for film exfoliation. This concept of epitaxial film growth using 2D materials is broadly divided into remote epitaxy and vdW epitaxy. For remote epitaxy to be possible, it is important that the 2D material is thin (typically monolayer or bilayer) such that the electrostatic potential of the substrate penetrates through the 2D material, providing the adatoms a sufficiently strong ionic potential to align them epitaxially on the substrate (142). If the 2D layer is thick or the substrate ionicity is not strong enough to penetrate through the 2D material (weak interaction between adatoms and the underlying substrate), then the adatoms will align randomly on the 2D material. This may result into a polycrystalline film or vdW epitaxy when the film has a preferential growth orientation on the 2D material. Therefore, a high ionicity of the substrate and good quality graphene are essential to achieve remote epitaxy (143, 144). On the other hand, vdW epitaxy is governed by vdW bonding between the film and the 2D substrate; the film then grows epitaxially following the crystallographic information of the underlying 2D material. The crystal quality of the grown film relies on the competition of surface energy and structural symmetry of the film and the 2D substrate. A suitable vdW substrate is essential to synthesize functional oxide membranes via vdW epitaxy. However, the vdW substrates for complex oxides are relatively limited (e.g., mica and graphene).

The graphene/perovskite oxide system is the most extensively studied for remote epitaxy, because of graphene's field transparency and the high ionicity of perovskite oxides. The quality of graphene plays a crucial role in remote epitaxy, with two primary transfer methods: the wet transfer of chemical vapor deposition (CVD)-grown graphene from a metal catalyst (145–147) and the semi-dry transfer of epitaxial graphene from SiC (148). The latter results in fewer defects, while CVD-grown graphene, being polycrystalline, typically contains more defects, which can hinder remote epitaxy

(143). Defects in graphene, such as cracks and holes, obstruct successful film exfoliation (65). Although SiC-based graphene shows promise, achieving defect-free transfers remains a challenge. Alternatively, graphene layers have been directly grown on single-crystal oxide substrates like SrTiO_3 (149, 150) and others (71, 151–154), but this method requires further refinement to address issues related to uniformity and controllable thickness (155, 156).

Another challenge to 2D layer-assisted lift-off involves the growth of complex oxide thin films on graphene. When using PLD, the laser energy must be carefully controlled to avoid damaging the graphene layer, which can result in the direct growth and poor film exfoliation. Typically, a low oxygen partial pressure below 10^{-6} torr and a substrate temperature of 700°C are used to protect the graphene layer (70). For MBE of complex oxides, additional oxygen sources like plasma or ozone can potentially oxidize the graphene. To prevent this, thicker buffer layers are grown on graphene in a low-pressure oxygen environment before introducing ozone into the chamber (157). Hybrid MBE has effectively circumvented this challenge. Using Sr supplied from an effusion cell and Ti-O from a TTIP precursor, SrTiO_3 (001) films were grown on graphene without an additional oxygen source (79). These films detached from graphene due to weak vdW bonds, leaving the graphene intact after exfoliation (79). However, remote epitaxy, vdW epitaxy, and pinhole-assisted epitaxy can all result in film exfoliation, although the precise mechanism driving film growth remains an active area of investigation. Pinhole-assisted epitaxy occurs when the film grows directly through cracks or holes in the 2D material, followed by lateral overgrowth. The growth mechanism on a 2D material-covered substrate depends on factors such as the material system, the quality of the 2D material, and the thin-film growth conditions (158). In many material systems, both remote epitaxy and pinhole-assisted epitaxy are considered possible mechanisms, largely because graphene often contains holes, leading to similar outcomes. As a result, systematic experimental studies are required to determine the true underlying growth mechanism.

Remote epitaxy of BaTiO_3 is demonstrated on a graphene-covered SrTiO_3 (001) substrate (159). The absence of lateral overgrowth of BaTiO_3 islands indicates remote epitaxy, ruling out pinhole-assisted epitaxy (159). However, both remote and vdW epitaxy may be possible because vdW epitaxy of BaTiO_3 on graphene also induces (001)-oriented growth (160). Thus, remote and vdW epitaxy should be carefully investigated to determine the true growth mechanism in the perovskite oxide/graphene/perovskite oxide (001) structure. Furthermore, to verify remote epitaxy, scanning transmission electron microscopy (STEM) is commonly used to observe the atomic arrangement of the epitaxial film on a 2D material-covered substrate, and electron backscatter diffraction (EBSD) is used to investigate film orientation. However, these results are necessary but not sufficient to confirm remote epitaxy. Additionally, these microscopic techniques only examine a limited film area. Therefore, complementary experiments and macroscopic studies are required to fully confirm remote epitaxy.

To summarize, remote epitaxy works well for materials with high ionicity and polarity, successfully producing membranes from a diverse range of materials, including III-V, III-N, II-VI, perovskites, and other complex oxides (64, 65, 141, 142, 144, 158, 161–166). Despite its versatility, several challenges remain for creating large-area membranes, particularly concerning the uniformity and quality of the graphene film. Additionally, the growth mechanism remains a key question that requires careful experimentation and characterization to resolve.

MECHANICAL LIFT-OFF (SPALLING)

Mechanical lift-off or spalling is a concept involving the use of stress at the edge of a film or substrate to aid lift-off, as shown in Fig. 3A (c). The stress causes the initiation of a crack at the edge of the crystal, which propagates parallel to its surface. The crack may be arrested, with the depth of the crack dependent on the fracture toughness of the material (167) and the stress field. In some cases, the entire crystal may naturally peel off from the substrate. This process occurs reproducibly in certain combinations of materials that fulfill the required properties. The process has been widely used for semiconductor layers (168, 169) and has also been applied to exfoliate complex oxides (65, 170–172). Typically, Ni is used as a stressor layer for spalling. For instance, $\text{Pb}(\text{Mg}_{1/3}\text{Nb}_{2/3})\text{O}_3$ - PbTiO_3 (PMN-PT) was deposited via sputtering on a SrRuO_3 film and exfoliated by applying a 3- to 5- μm Ni stressor layer, resulting in a PMN-PT membrane (65). In the case of $\text{LaAlO}_3/\text{SrTiO}_3$, the LaAlO_3 film serves not only as a functional film but also as a stressor layer due in part to the lattice mismatch (+3.12%), leading to spalling of $\text{LaAlO}_3/\text{SrTiO}_3$ (170). The membrane size was controlled by Ar^+ -ion milling pre-patterned substrate (lateral size: 2 μm to 20 μm). Furthermore, the $\text{LaAlO}_3/\text{SrTiO}_3$ membrane was transferred to a SiO_2/Si substrate and exhibited 2D superconducting electron gas, demonstrating the potential for integrating functional oxide membranes with Si-based electronics (172).

Conceptually, mechanical lift-off depends more on the material systems than on the growth techniques because the additional stressor layer must be deposited on the grown film for exfoliation. Although this may seem like a universal method for creating free-standing membranes, spalling works for a limited combination of materials with certain mechanical properties. So far, only a few oxide membranes (e.g., PMN-PT and $\text{LaAlO}_3/\text{SrTiO}_3$) have been synthesized using this method. Given that the fracture is fundamentally sensitive to minor defects, it is difficult to manage crack propagation, leading to challenges in controlling the thickness and surface roughness of a free-standing membrane (156). For future applications of free-standing oxide membranes, spalling might be useful for specific materials, but there are still questions regarding the available oxide systems, scalability of the membrane, and transfer/integration method.

MEMBRANE EXFOLIATION AND TRANSFER PROCESSES

Once a membrane growth method is selected—whether chemical lift-off or 2D layer-assisted lift-off—careful exfoliation and transfer of the film onto the desired host substrate is crucial for ensuring the quality and integrity of the transferred film. This step is essential for achieving the desired film properties and performance in the final device. Currently, the process of exfoliation and transfer for oxide membranes is tedious and involves multiple steps, making it difficult to generalize across all oxide systems (12). This section reviews the exfoliation and transfer processes involved in chemical lift-off and remote epitaxy, addressing their associated challenges and opportunities. It also explores potential solutions to enhance the transfer yield of membranes with atomically smooth surfaces, aiming to streamline the process and improve reproducibility for a broader range of oxide materials.

Fabricating a membrane that is tens of nanometers thick using the chemical lift-off method requires mechanical support during the sacrificial layer etching process. This support is later removed to

achieve a pristine membrane on the host substrate, but the transfer and etching process can introduce defects and residues. To mitigate these issues, one approach is to use supporting layers, such as silicone-coated polyethylene terephthalate (PET), polyimide (PI) tape, thermal release tape, or polydimethylsiloxane (PDMS), which are applied on top of the functional film. These supporting layers provide the necessary flexibility and stretchability for various applications (Fig. 3B, a). Previously, membranes of $\text{YBa}_2\text{Cu}_3\text{O}_{7-x}$, SrTiO_3 , $\text{La}_{0.7}\text{Sr}_{0.3}\text{MnO}_3$, $\text{SrTiO}_3/\text{La}_{0.7}\text{Sr}_{0.3}\text{MnO}_3$ superlattices, BiFeO_3 , SrRuO_3 , and BaTiO_3 (3, 4, 109) were successfully transferred by a supporting layer. Some examples are shown in Fig. 3C (a and b).

Alternatively, a mechanical supporting layer such as polymethyl methacrylate (PMMA), cellulose acetate butyrate (CAB), Au, and Pt (44, 49, 173–175) can be coated on top of the film, as shown in Fig. 3B (b). However, etching in acetone to remove PMMA can be aggressive, leading to membrane cracking. One interesting approach to circumvent this issue is to use a thermal release tape with a square cut ($\sim 3 \text{ mm}^2$) on top of PMMA. The membrane in this square cut frame is fully transferred (110, 176). SrRuO_3 membrane transferred using this method is shown in Fig. 3C (c). A limitation of this approach is that some organic residues on the membrane surface are unavoidable. CAB is perhaps a better choice due to its controllable adhesion to oxides, flexibility, and high modulus, leading to negligible polymer residue after dissolving in acetone (26). A millimeter-scale SrTiO_3 film was transferred onto a TiN/Si substrate using CAB, as shown in Fig. 3C (d). Alternative to a polymer-based supporting layer, a ~ 1 - μm -thick Ni stressor layer with a Ti adhesion layer has also been used on top of the functional film. A thermal release tape is then applied on top of the Ni stressor layer, facilitating the exfoliation and transfer process to the target substrate. The Ti adhesion and Ni stressor layer can be removed using a buffered oxide etchant and FeCl_3 (177), respectively, or the Ni/Ti/membrane structure can be used directly for characterization (66). This method has been effective for remote and vdW epitaxially grown films, and pinhole-assisted epitaxy in certain material systems (178). Figure 3C (e) shows transferred functional $\text{BaTiO}_{3-\delta}$ membrane on a $\text{Au}/\text{Cr}/\text{PI}$ layer using a Ni stressor layer (65). In spalling method, deposited functional films can also serve as a stressor layer (and a supporting layer). A representative $\text{LaAlO}_3/\text{SrTiO}_3$ membrane obtained on a Si substrate is shown in Fig. 3C (f).

To avoid residues and contaminants, the film can be exfoliated and transferred without a supporting layer (Fig. 3C, c) (42, 179, 180). This method involves scooping the free-standing membrane onto a host substrate after dissolving the sacrificial layer in water. A large-area (millimeter-scale) SrRuO_3 and $\text{Hf}_{0.5}\text{Zr}_{0.5}\text{O}_2$ films were transferred onto PET and SiO_2/Si substrates, respectively, without the use of a supporting layer (Fig. 3C, g and h).

An optimized exfoliation and transfer process is important. For instance, slower dissolution speed and coherently strained films produce larger lateral size membranes (115). The sign of the strain on the film also affects membrane size; tensile-strained films induce cracks during the release process, whereas compressive-strained films lead to wrinkles (181). Films under compressive strain are advantageous for large membranes as wrinkles can be flattened during transfer. Additionally, the thickness of the polymer layer influences membrane size and can be controlled. Thinner polymer layers help increase membrane size by adapting to changes during the release process (181).

To reduce cracks in membranes, an amorphous Al_2O_3 capping layer was used to show crack suppression in La-SrSnO_3 membranes

using the $\text{Sr}_3\text{Al}_2\text{O}_6$ sacrificial layer (182). The high Young's modulus and high crack resistance of Al_2O_3 help in increasing the strength of fragile membrane, thus helping in reducing wrinkles and cracks in the transferred membrane (182).

SUMMARY AND OUTLOOK

Free-standing membranes enable the creation of unique device architectures that traditional methods cannot achieve. They allow for the integration of optimal materials for each layer, facilitating the development of artificial, nonequilibrium, stretched, wrinkled, and symmetry-mismatched heterostructures. These membranes can also be flexible and stretchable, meeting the needs of next-generation quantum information devices and flexible electronics. Techniques like PLD and MBE (including hybrid MBE), known for producing thin films with exceptional electronic properties, can be used to create single-crystal, few-atomic-layer membranes with unique properties not found in bulk materials. These can be stacked to form unusual bicrystal interfaces. Combining an appropriate thin-film growth method with efficient membrane synthesis, exfoliation and transfer is expected to address the vertical integration needs of the microelectronics industry. Additionally, the rich physics of functional oxides has spurred interest in integrating these with 2D vdW materials (183) like graphene, hBN, and TMDCs.

Similarly, there is growing interest in combining 3D/3D membranes of functional oxides. Advances in the fabrication of 2D/3D, 3D/3D, and stacked mono-, bi-, and trilayers have led to the emergence of fields such as Moirétronics, stacktronics, and twistronics. When two layers are rotated and periodically stacked, they create a Moiré superlattice, with the Moiré length (λ) determined by the angle (θ) between layers A and B, as shown in the center of Fig. 4. This raises fundamental questions about how the electronic structure and properties change when 3D/3D materials form Moiré patterns, are stacked at specific angles, or are twisted to create chiral heterostructures. Figure 4 outlines a future outlook in stacking and Moiré engineering, categorized into five interrelated topics: bonding/structure, quasicrystals, electronic structure, properties, and unique architectures.

From a bonding and structure perspective, stacking 3D materials with dangling bonds raises several questions. These include consideration of orbital hybridization, bonding between layers, optimal angles for bonding, strain resulting from atomic order mismatch, formation of dislocations, periodic wrinkling, occurrence of point defects, and potential structural reconstruction. These factors are depicted in the center-right octagon of Fig. 4. For example, Li *et al.* (26) demonstrated that covalent or ionic bonds are formed at the interfaces of two 3D layers following a post-annealing process at 650°C. Once these strong covalent or ionic bonds are established, controlling the angle becomes challenging, leading to difficulties in angle adjustment or inability to perform in situ rotation. Additionally, preferred or possible twist angles may exist at 3D/3D interfaces due to the presence of strong bonds. Moreover, topological defects like screw dislocations (184) and point defects can be studied and engineered in these nanomembranes. Confirmation of the occurrence of structural reconstruction, which affects the properties of materials, will be crucial in 3D/3D stacking as well.

The abovementioned structural changes at the interface will likely be accompanied by unusual electronic structures (center-left octagon

of Fig. 4). These variations could affect several aspects including the band structure, correlation strength, phonon dispersion, band topology, polariton behavior, and excitons. Such variations may potentially lead to the emergence of exotic phenomena, such as flat bands and interlayer excitons, akin to those demonstrated in Moiré structures of 2D materials. Further, the unexpected electronic properties such as superconductivity, ferroelectricity, ferromagnetism, and insulator/metal transitions can be exhibited, or their properties can be altered (as illustrated in the top-left octagon of Fig. 4). Electronic, magnetic, and spin properties are extremely sensitive to such modifications at the interface, and the controlled manipulation, tuning, and knitting of the interfaces may produce intriguing properties (185).

3D membranes have the potential to create origami-inspired nanostructures (186), which are highly sought after in space technologies and health care technologies and are often used as implants. Unlike conventional materials used in health care, 3D oxide materials with multifunctionalities can now be integrated and tested as devices in pacemakers, as well as in catheters for treating brain aneurysms. Nanomembranes possessing polar texture (187) or vortex/antivortex structures (188) can serve as virtual substrates to induce chirality into a material of choice. Additionally, twisted superlattices can be designed to provide an additional tuning knob for controlling properties in 3D/3D Moiré structures, serving as unique architectures. Further, it has been shown that, while in epitaxial systems strain is typically limited to <2%, stretching perfect membranes can achieve extreme strain states (189), which in turn is a powerful tool to manipulate the properties of the material (190). The application of uniform strain can break rotational and translation symmetries, while strain gradients can break inversion symmetry (189). Similarly, the strain at the Moiré interface could cause breaking symmetries. Specifically, the strain gradient may create polar distortions, Dzyaloshinskii-Moriya interaction (DMI), chiral spin textures, tunable Weyl nodes, nonlinear optical response, and Rashba splitting.

Since the rotation angles between the 3D layers are manipulable, a rich design space can be envisioned, such as quasicrystals (bottom octagon of Fig. 4) and superlattices/artificial architecture (top-right octagon of Fig. 4). Quasicrystals are ordered but aperiodic structures having Fourier transforms consisting of discrete sharp peaks, which have rotational symmetry orders other than the two-, three-, four-, and sixfold orders that are found in crystals (191). By stacking multiple layers of membranes, quasicrystals can be obtained, providing a way to fabricate them, and a challenge to mathematically understand them and to find intriguing physical properties. Moreover, unlike 2D materials that are largely limited to hexagonal lattices, 3D materials can have hexagonal, square, and triangular lattices, which give more design freedom. For instance, an eightfold quasicrystal can be achieved by superposing two square lattices with 45° relative rotation angle, which is not realizable by stacking hexagonal lattices. While researchers have made initial strides in 3D oxide membrane synthesis, release, and stacking, innovative approaches are required to experimentally characterize and theoretically model these structures and their associated properties. Both experimental and theoretical research is needed to explore the unusual properties of these structures. Additionally, developing extensive predictive theories and models for stacking and twisting membranes will be crucial for accelerating scientific discoveries in this field.

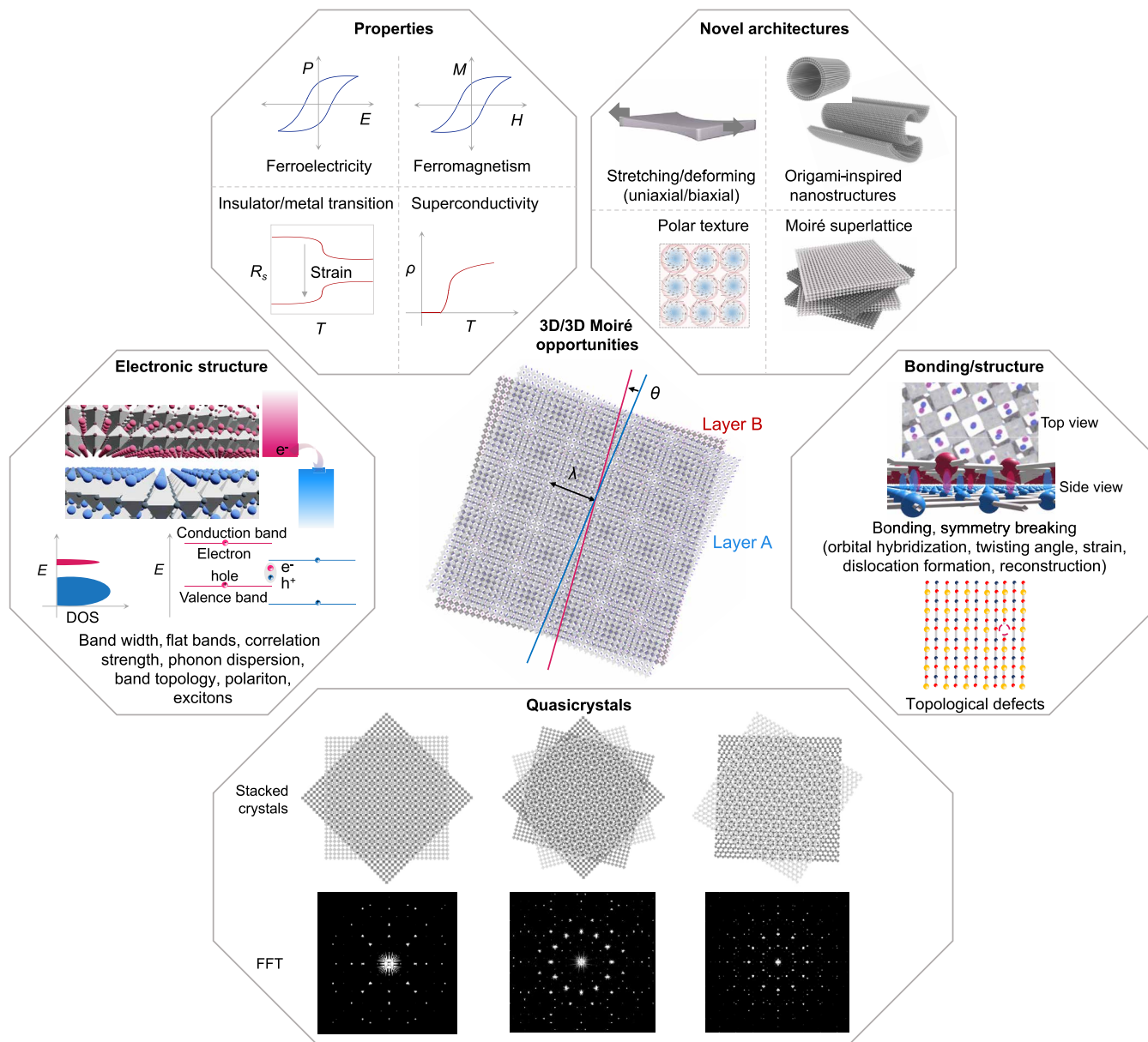


Fig. 4. Outlook for oxide membranes for twistronics/Moirétronics/stacktronics. The center panel shows a Moiré pattern formed by stacking layer A over layer B. θ is the twist angle, and λ is the length scale of the moiré superlattice. First octagon (middle left) focuses on the change in electronic structure as two membranes are stacked. The change in band structure is often observed in twisted layers, giving rise, in some cases, to flat bands. Others include correlation strength, phonon dispersion, band topology, generation of polaritons, and excitons. Second octagon (top left) focuses on the modification in electronic properties like ferroelectricity, ferromagnetism, insulator-metal transition, and superconductivity. Third octagon (top right) covers the physics enabled by unique architectures created by free-standing membranes. For example, the membrane can be stretched to achieve extreme strain states and deformed into origami-inspired 3D architectures. Polar texture present in stacked membranes and Moiré superlattices is a platform as a virtual substrate. Fourth octagon (middle right) is about the bonding and symmetry breaking as a result of stacking two layers. They can lead to changes in hybridization states of the orbital as a result of bond formation. The layers may also be strained or reconstructed into a low-energy state. Further, the study of topological defects is possible in free-standing 3D oxides. Finally, the fifth octagon (bottom) focuses on the design of quasicrystalline interfaces created by stacking and rotating 3D oxide layers.

Downloaded from https://www.science.org at DOE Office of Science on December 18, 2024

REFERENCES AND NOTES

- R.-C. Peng, X. Cheng, B. Peng, Z. Zhou, L.-Q. Chen, M. Liu, Domain patterns and super-elasticity of freestanding BiFeO₃ membranes via phase-field simulations. *Acta Mater.* **208**, 116689 (2021).
- H. Elangovan, M. Barzilay, S. Seremi, N. Cohen, Y. Jiang, L. W. Martin, Y. Ivry, Giant superelastic piezoelectricity in flexible ferroelectric BaTiO₃ membranes. *ACS Nano* **14**, 5053–5060 (2020).
- G. Dong, S. Li, M. Yao, Z. Zhou, Y.-Q. Zhang, X. Han, Z. Luo, J. Yao, B. Peng, Z. Hu, H. Huang, T. Jia, J. Li, W. Ren, Z.-G. Ye, X. Ding, J. Sun, C.-W. Nan, L.-Q. Chen, J. Li, M. Liu, Super-elastic ferroelectric single-crystal membrane with continuous electric dipole rotation. *Science* **366**, 475–479 (2019).
- B. Peng, R.-C. Peng, Y.-Q. Zhang, G. Dong, Z. Zhou, Y. Zhou, T. Li, Z. Liu, Z. Luo, S. Wang, Y. Xia, R. Qiu, X. Cheng, F. Xue, Z. Hu, W. Ren, Z.-G. Ye, L.-Q. Chen, Z. Shan, T. Min, M. Liu, Phase transition enhanced superior elasticity in freestanding single-crystalline multiferroic BiFeO₃ membranes. *Sci. Adv.* **6**, eaba5847 (2020).
- S.-I. Kim, H.-J. Choi, G. Lee, C. J. Roh, I. Jung, S. Y. Jung, R. Ning, S. O. Won, H. J. Chang, J. S. Lee, S. K. Kim, J.-S. Kim, C.-Y. Kang, J.-W. Choi, S.-H. Baek, 3D architectures of single-crystalline complex oxides. *Mater. Horiz.* **7**, 1552–1557 (2020).
- V. Harbola, Y. Wu, F. V. E. Hensling, H. Wang, P. A. Van Aken, J. Mannhart, Vector substrates: Idea, design, and realization. *Adv. Funct. Mater.* **34**, 2306289 (2024).
- H. Li, S. Yun, A. Chikina, V. Rosendal, T. Tran, E. Brand, C. H. Christoffersen, N. C. Plumb, M. Shi, N. Pryds, M. Radovic, Transition metal-oxide nanomembranes assembly by direct heteroepitaxial growth. *Adv. Funct. Mater.* **34**, 2313236 (2024).
- F. M. Chiabrera, S. Yun, Y. Li, R. T. Dahm, H. Zhang, C. K. R. Kirchert, D. V. Christensen, F. Trier, T. S. Jespersen, N. Pryds, Freestanding perovskite oxide films: Synthesis, challenges, and properties. *Ann. Phys.* **534**, 2200084 (2022).
- J. A. Rogers, M. G. Lagally, R. G. Nuzzo, Synthesis, assembly and applications of semiconductor nanomembranes. *Nature* **477**, 45–53 (2011).
- P.-C. Wu, Y.-H. Chu, Development of oxide heteroepitaxy for soft technology. *J. Mater. Chem. C* **6**, 6102–6117 (2018).
- M. Yao, Y. Cheng, Z. Zhou, M. Liu, Recent progress on the fabrication and applications of flexible ferroelectric devices. *J. Mater. Chem. C* **8**, 14–27 (2020).
- Y. Bitla, Y.-H. Chu, Van der Waals oxide heteroepitaxy for soft transparent electronics. *Nanoscale* **12**, 18523–18544 (2020).
- A. G. Ricciardulli, S. Yang, J. H. Smet, M. Saliba, Emerging perovskite monolayers. *Nat. Mater.* **20**, 1325–1336 (2021).
- O. Dubnack, F. A. Müller, Oxidic 2D materials. *Materials* **14**, 5213 (2021).
- L. Han, C. Addiego, S. Prokhorenko, M. Wang, H. Fu, Y. Nahas, X. Yan, S. Cai, T. Wei, Y. Fang, H. Liu, D. Ji, W. Guo, Z. Gu, Y. Yang, P. Wang, L. Bellaiche, Y. Chen, D. Wu, Y. Nie, X. Pan, High-density switchable skyrmion-like polar nanodomains integrated on silicon. *Nature* **603**, 63–67 (2022).
- K. Kerman, S. Ramanathan, Complex oxide nanomembranes for energy conversion and storage: A review. *J. Mater. Res.* **29**, 320–337 (2014).
- D. Pesquera, A. Fernández, E. Khestanova, L. W. Martin, Freestanding complex-oxide membranes. *J. Phys. Condens. Matter* **34**, 383001 (2022).
- D. Pesquera, E. Parsonnet, A. Qualls, R. Xu, A. J. Gubser, J. Kim, Y. Jiang, G. Velarde, Y. Huang, H. Y. Hwang, R. Ramesh, L. W. Martin, Beyond substrates: Strain engineering of ferroelectric membranes. *Adv. Mater.* **32**, e2003780 (2020).
- Y. Zhang, J. Li, K. Yang, F. Zheng, Y. Zhou, Y. Zhang, Y. Hui, Y.-Q. Wang, J. Zhu, J. Zhang, Y. Hao, M. Yang, T. Li, J. Zhao, H. H. Ma, Room-temperature electric field-induced out-of-plane ferroelectric polarization in strain-free freestanding 2D SrTiO₃ membranes. *APL Mater.* **11**, 041103 (2023).
- Y. Wang, Y. Zhu, S. Chen, D. Rong, Q. Jin, E.-J. Guo, Lateral strain tailoring in manganese homostructures assisted by atomic-flat freestanding membranes. *Nano Res.* **16**, 7829–7836 (2023).
- L. Han, Y. Fang, Y. Zhao, Y. Zang, Z. Gu, Y. Nie, X. Pan, giant uniaxial strain ferroelectric domain tuning in freestanding PbTiO₃ films. *Adv. Mater. Interfaces* **7**, 1901604 (2020).
- V. Harbola, S. Crossley, S. S. Hong, D. Lu, Y. A. Birkhölzer, Y. Hikita, H. Y. Hwang, Strain gradient elasticity in SrTiO₃ membranes: Bending versus stretching. *Nano Lett.* **21**, 2470–2475 (2021).
- G. Dong, S. Li, T. Li, H. Wu, T. Nan, X. Wang, H. Liu, Y. Cheng, Y. Zhou, W. Qu, Y. Zhao, B. Peng, Z. Wang, Z. Hu, Z. Luo, W. Ren, S. J. Pennycook, J. Li, J. Sun, Z. Ye, Z. Jiang, Z. Zhou, X. Ding, T. Min, M. Liu, Periodic wrinkle-patterned single-crystalline ferroelectric oxide membranes with enhanced piezoelectricity. *Adv. Mater.* **32**, e2004477 (2020).
- J. Fompeyrine, R. Berger, H. P. Lang, J. Perret, E. Mächler, C. Gerber, J.-P. Locquet, Local determination of the stacking sequence of layered materials. *Appl. Phys. Lett.* **72**, 1697–1699 (1998).
- Q. Wang, H. Liu, B. He, J. Qi, D. Wang, H. Xu, N. Zhang, J. Wang, Y. Chen, Z. Wang, Z. Wang, X. Qi, L. Zheng, M. Feng, W. Lü, S. Yan, Enhanced oxygen evolution reaction by stacking single-crystalline freestanding SrRuO₃. *Appl. Catal. B* **317**, 121781 (2022).
- Y. Li, C. Xiang, F. M. Chiabrera, S. Yun, H. Zhang, D. J. Kelly, R. T. Dahm, C. K. R. Kirchert, T. E. L. Cozannet, F. Trier, D. V. Christensen, T. J. Booth, S. B. Simonsen, S. Kadhkodzadeh, T. S. Jespersen, N. Pryds, Stacking and twisting of freestanding complex oxide thin films. *Adv. Mater.* **34**, e2203187 (2022).
- Y. Cao, V. Fatemi, S. Fang, K. Watanabe, T. Taniguchi, E. Kaxiras, P. Jarillo-Herrero, Unconventional superconductivity in magic-angle graphene superlattices. *Nature* **556**, 43–50 (2018).
- J. Shen, Z. Dong, M. Qi, Y. Zhang, C. Zhu, Z. Wu, D. Li, Observation of moiré patterns in twisted stacks of bilayer perovskite oxide nanomembranes with various lattice symmetries. *ACS Appl. Mater. Interfaces* **14**, 50386–50392 (2022).
- X. Lu, P. Stepanov, W. Yang, M. Xie, M. A. Aamir, I. Das, C. Urgell, K. Watanabe, T. Taniguchi, G. Zhang, A. Bachtold, A. H. MacDonald, D. K. Efetov, Superconductors, orbital magnets and correlated states in magic-angle bilayer graphene. *Nature* **574**, 653–657 (2019).
- P.-C. Wu, C.-C. Wei, Q. Zhong, S.-Z. Ho, Y.-D. Liou, Y.-C. Liu, C.-C. Chiu, W.-Y. Tzeng, K.-E. Chang, Y.-W. Chang, J. Zheng, C.-F. Chang, C.-M. Tu, T.-M. Chen, C.-W. Luo, R. Huang, C.-G. Duan, Y.-C. Chen, C.-Y. Kuo, J.-C. Yang, Twisted oxide lateral homostructures with conjunction tunability. *Nat. Commun.* **13**, 2565 (2022).
- Y. Lun, S. Xu, X. Wang, J. Hong, Flexoelectricity in self-rolling freestanding heterogeneous films. *Int. J. Solids Struct.* **271–272**, 112223 (2023).
- J. L. MacManus-Driscoll, M. P. Wells, C. Yun, J.-W. Lee, C.-B. Eom, D. G. Schlom, New approaches for achieving more perfect transition metal oxide thin films. *APL Mater.* **8**, 040904 (2020).
- H. Cao, X. Yan, Y. Li, L. Stan, W. Chen, N. P. Guisinger, H. Zhou, D. D. Fong, Enhancing the metal-insulator transition in VO₂ heterostructures with graphene interlayers. *Appl. Phys. Lett.* **121**, 081601 (2022).
- S. A. Chambers, Epitaxial growth and properties of doped transition metal and complex oxide films. *Adv. Mater.* **22**, 219–248 (2010).
- W. S. Choi, C. M. Rouleau, S. S. A. Seo, Z. Luo, H. Zhou, T. T. Fister, J. A. Eastman, P. H. Fuoss, D. D. Fong, J. Z. Tischler, G. Eres, M. F. Chisholm, H. N. Lee, Atomic layer engineering of perovskite oxides for chemically sharp heterointerfaces. *Adv. Mater.* **24**, 6423–6428 (2012).
- S. Chen, Q. Jin, S. Lin, H. Hong, T. Cui, D. Rong, G. Song, S. Wang, K. Jin, Q. Zheng, E.-J. Guo, Synthesis of functional nitride membranes using sacrificial water-soluble BaO layers. *J. Appl. Phys.* **133**, 045303 (2023).
- J. Shen, B. K. Tsai, K. Xu, A. Shang, J. P. Barnard, Y. Zhang, R. Tripathi, Z. Chen, X. Zhang, H. Wang, A generalized synthesis method for freestanding multiferroic two-dimensional layered supercell oxide films via a sacrificial buffer layer. *Nano Res.* **16**, 10559–10566 (2023).
- S. R. Bakaul, C. R. Serrao, M. Lee, C. W. Yeung, A. Sarker, S.-L. Hsu, A. K. Yadav, L. Dedon, L. You, A. I. Khan, J. D. Clarkson, C. Hu, R. Ramesh, S. Salahuddin, Single crystal functional oxides on silicon. *Nat. Commun.* **7**, 10547 (2016).
- R. Xu, K. J. Crust, V. Harbola, R. Arras, K. Y. Patel, S. Prosandeev, H. Cao, Y. Shao, P. Behera, L. Caretta, W. J. Kim, A. Khandelwal, M. Acharya, M. M. Wang, Y. Liu, E. S. Barnard, A. Raja, L. W. Martin, X. W. Gu, H. Zhou, R. Ramesh, D. A. Muller, L. Bellaiche, H. Y. Hwang, Size-induced ferroelectricity in antiferroelectric oxide membranes. *Adv. Mater.* **35**, 2210562 (2023).
- C. Jin, Y. Zhu, X. Li, F. An, W. Han, Q. Liu, S. Hu, Y. Ji, Z. Xu, S. Hu, M. Ye, G. Zhong, M. Gu, L. Chen, Super-flexible freestanding BiMnO₃ membranes with stable ferroelectricity and ferromagnetism. *Adv. Sci.* **8**, e2102178 (2021).
- W. Hou, M. Yao, R. Qiu, Z. Wang, Z. Zhou, K. Shi, J. Pan, M. Liu, J. Hu, Epitaxial lift-off of flexible single-crystal magnetite thin films with tunable magnetic performances by mechanical deformation. *J. Alloys Compd.* **887**, 161470 (2021).
- H. Zhong, M. Li, Q. Zhang, L. Yang, R. He, F. Liu, Z. Liu, G. Li, Q. Sun, D. Xie, F. Meng, Q. Li, M. He, E. Guo, C. Wang, Z. Zhong, X. Wang, L. Gu, G. Yang, K. Jin, P. Gao, C. Ge, Large-Scale Hf_{0.5}Zr_{0.5}O₂ membranes with robust ferroelectricity. *Adv. Mater.* **34**, e2109889 (2022).
- S. Lindemann, J. Irwin, G.-Y. Kim, B. Wang, K. Eom, J. Wang, J. Hu, L.-Q. Chen, S.-Y. Choi, C.-B. Eom, M. S. Rzechowski, Low-voltage magnetoelectric coupling in membrane heterostructures. *Sci. Adv.* **7**, eabh2294 (2021).
- T. Mizuyama, H. Nishikawa, Effect of platinum buffer layer on the fabrication process of flexible ferroelectric epitaxial thin films. *IEEE Trans. Electron. Inf. Syst.* **142**, 1060–1063 (2023).
- J. Wang, Y. Liang, Y. Wang, S. Yang, X. Zhang, X. Huang, Y. Wang, Z. Liang, J. Ma, H. Zhang, Q. Chen, J. Ma, Y. Lin, L. Wu, Refreshment of SrTiO₃ substrate for layer peeling-off using sacrificial Sr₃Al₂O₆. *Adv. Mater. Interfaces* **10**, 2202111 (2023).
- M. Lee, J. R. Renshof, K. J. Van Zeggeren, M. J. A. Houmes, E. Lesne, M. Šiškins, T. C. Van Thiel, R. H. Guis, M. R. Van Blankenstein, G. J. Verbiest, A. D. Caviglia, H. S. J. Van Der Zant, P. G. Steeneken, Ultrathin piezoelectric resonators based on graphene and free-standing single-crystal BaTiO₃. *Adv. Mater.* **34**, e2204630 (2022).
- H. Liu, W. Zhu, Q. Mao, B. Peng, Y. Xu, G. Dong, B. Chen, R. Peng, Y. Zhao, Z. Zhou, S. Yang, H. Huang, M. Liu, Single-Crystalline BaZr_{0.8}Ti_{0.2}O₃ membranes enabled high energy density in PEL-based composites for high-temperature electrostatic capacitors. *Adv. Mater.* **35**, e2300962 (2023).

48. H. Liu, H. Yuan, G. Dong, K. Wu, G. Liu, J. Sun, Z. Zhou, M. Liu, Tunable friction properties of periodic wrinkled BaTiO₃ membranes. *Adv. Mater. Interfaces* **9**, 2102316 (2022).
49. J. Bouaziz, C. Cancellieri, B. Rheingans, L. P. H. Jeurgens, F. La Mattina, Advanced epitaxial lift-off and transfer procedure for the fabrication of high-quality functional oxide membranes. *Adv. Mater. Interfaces* **10**, 2201458 (2023).
50. Y. Guo, B. Peng, R. Qiu, G. Dong, Y. Yao, Y. Zhao, Z. Zhou, M. Liu, Self-rolling-up enabled ultrahigh-density information storage in freestanding single-crystalline ferroic oxide films. *Adv. Funct. Mater.* **33**, 2213668 (2023).
51. J. Shiogai, A. Tsukazaki, Superconducting FeSe membrane synthesized by etching of water-soluble Sr₃Al₂O₇ layer. *Appl. Phys. Lett.* **122**, 052602 (2023).
52. W. Zhou, W. Han, Y. Yang, L. Shu, Q. Luo, Y. Ji, C. Jin, Y. Zhang, J. Song, M. Ye, Q. Liu, S. Hu, L. Chen, Synthesis of freestanding perovskite oxide thin films by using brownmillerite SrCo₂O₇ as a sacrificial layer. *Appl. Phys. Lett.* **122**, 062901 (2023).
53. P. Zhang, B. He, J. Guo, Q. Wang, Y. Han, C. Shi, Y. Chen, H. Fang, J. Wang, S. Yan, W. Lü, Extreme enhanced curie temperature and perpendicular exchange bias in freestanding ferromagnetic superlattices. *ACS Appl. Mater. Interfaces* **15**, 17309–17316 (2023).
54. Z. Lu, J. Liu, J. Feng, X. Zheng, L. Yang, C. Ge, K. Jin, Z. Wang, R.-W. Li, Synthesis of single-crystal La_{0.67}Sr_{0.33}MnO₃ freestanding films with different crystal-orientation. *APL Mater.* **8**, 051105 (2020).
55. D. K. Lee, Y. Park, H. Sim, J. Park, Y. Kim, G.-Y. Kim, C.-B. Eom, S.-Y. Choi, J. Son, Heterogeneous integration of single-crystalline rutile nanomembranes with steep phase transition on silicon substrates. *Nat. Commun.* **12**, 5019 (2021).
56. P. Su, H. Wen, Y. Zhang, C. Tan, X. Zhong, Y. Wu, H. Song, Y. Zhou, Y. Li, M. Liu, J. Wang, Super-flexibility in freestanding single-crystal SrRuO₃ conductive oxide membranes. *ACS Appl. Electron. Mater.* **4**, 2987–2992 (2022).
57. J. Park, J. H. Shin, K. Song, Y.-J. Kim, H.-B. Jang, H. Lee, H.-S. Sim, C.-H. Yang, Non-Ohmic conduction in exfoliated La_{0.7}Ca_{0.3}MnO₃ thin films. *Appl. Phys. Lett.* **116**, 022401 (2020).
58. P. Singh, A. Swartz, D. Lu, S. S. Hong, K. Lee, A. F. Marshall, K. Nishio, Y. Hikita, H. Y. Hwang, Large-area crystalline BaSnO₃ membranes with high electron mobilities. *ACS Appl. Electron. Mater.* **1**, 1269–1274 (2019).
59. Y.-W. Chang, P.-C. Wu, J.-B. Yi, Y.-C. Liu, Y. Chou, Y.-C. Chou, J.-C. Yang, A fast route towards freestanding single-crystalline oxide thin films by using YBa₂Cu₃O_{7-x} as a sacrificial layer. *Nanoscale Res. Lett.* **15**, 172 (2020).
60. Q. Shi, E. Parsonnet, X. Cheng, N. Fedorova, R.-C. Peng, A. Fernandez, A. Qualls, X. Huang, X. Chang, H. Zhang, D. Pesquera, S. Das, D. Nikonov, I. Young, L.-Q. Chen, L. W. Martin, Y.-L. Huang, J. Íñiguez, R. Ramesh, The role of lattice dynamics in ferroelectric switching. *Nat. Commun.* **13**, 1110 (2022).
61. V. Harbola, R. Xu, S. Crossley, P. Singh, H. Y. Hwang, Fracture and fatigue of thin crystalline SrTiO₃ membranes. *Appl. Phys. Lett.* **119**, 053102 (2021).
62. S. Leontsev, P. J. Shah, H. S. Kum, J. L. McChesney, F. M. Rodolakis, M. Van Veenendaal, M. Velez, R. Rao, D. Haskel, J. Kim, A. N. Reed, M. R. Page, Functional properties of Yttrium Iron Garnet thin films on graphene-coated Gd₃Ga₅O₁₂ for remote epitaxial transfer. *J. Magn. Magn. Mater.* **556**, 169440 (2022).
63. R. Jia, H. S. Kum, X. Sun, Y. Guo, B. Wang, P. Fang, J. Jiang, D. Gall, T.-M. Lu, M. Washington, J. Kim, J. Shi, Van der Waals epitaxy and remote epitaxy of LiNbO₃ thin films by pulsed laser deposition. *J. Vac. Sci. Technol. A* **39**, 040405 (2021).
64. Y. Guo, X. Sun, J. Jiang, B. Wang, X. Chen, X. Yin, W. Qi, L. Gao, L. Zhang, Z. Lu, R. Jia, S. Pendse, Y. Hu, Z. Chen, E. Wertz, D. Gall, J. Feng, T.-M. Lu, J. Shi, A reconfigurable remotely epitaxial VO₂ electrical heterostructure. *Nano Lett.* **20**, 33–42 (2020).
65. H. S. Kum, H. Lee, S. Kim, S. Lindemann, W. Kong, K. Qiao, P. Chen, J. Irwin, J. H. Lee, S. Xie, S. Subramanian, J. Shim, S.-H. Bae, C. Choi, L. Ranno, S. Seo, S. Lee, J. Bauer, H. Li, K. Lee, J. A. Robinson, C. A. Ross, D. G. Schlom, M. S. Rzchowski, C.-B. Eom, J. Kim, Heterogeneous integration of single-crystalline complex-oxide membranes. *Nature* **578**, 75–81 (2020).
66. L. Dai, J. Zhao, J. Li, B. Chen, S. Zhai, Z. Xue, Z. Di, B. Feng, Y. Sun, Y. Luo, M. Ma, J. Zhang, S. Ding, L. Zhao, Z. Jiang, W. Luo, Y. Quan, J. Schwarzkopf, T. Schroeder, Z.-G. Ye, Y.-H. Xie, W. Ren, G. Niu, Highly heterogeneous epitaxy of flexoelectric BaTiO_{3-δ} membrane on Ge. *Nat. Commun.* **13**, 2990 (2022).
67. A. Koma, K. Yoshimura, Ultrathin interfaces grown with Van der Waals epitaxy. *Surf. Sci.* **174**, 556–560 (1986).
68. A. Koma, Van der Waals epitaxy for highly lattice-mismatched systems. *J. Cryst. Growth* **201–202**, 236–241 (1999).
69. Y. Yang, G. Yuan, Z. Yan, Y. Wang, X. Lu, J. Liu, Flexible, semitransparent, and inorganic resistive memory based on BaTi_{0.95}Co_{0.05}O₃ film. *Adv. Mater.* **29**, 1700425 (2017).
70. S. A. Lee, J.-Y. Hwang, E. S. Kim, S. W. Kim, W. S. Choi, Highly oriented SrTiO₃ thin film on graphene substrate. *ACS Appl. Mater. Interfaces* **9**, 3246–3250 (2017).
71. J.-Y. Hwang, Y.-M. Kim, K. H. Lee, H. Ohta, S. W. Kim, Te monolayer-driven spontaneous van der Waals epitaxy of two-dimensional pnictogen chalcogenide film on sapphire. *Nano Lett.* **17**, 6140–6145 (2017).
72. J. Liu, Y. Feng, R. Tang, R. Zhao, J. Gao, D. Shi, H. Yang, Mechanically tunable magnetic properties of flexible SrRuO₃ epitaxial thin films on mica substrates. *Adv. Electron. Mater.* **4**, 1700522 (2018).
73. W. Nunn, T. K. Truttman, B. Jalan, A review of molecular-beam epitaxy of wide bandgap complex oxide semiconductors. *J. Mater. Res.* **36**, 4846–4864 (2021).
74. A. B. Mei, L. Miao, M. J. Wahila, G. Khalsa, Z. Wang, M. Barone, N. J. Schreiber, L. E. Noskin, H. Paik, T. E. Tiwald, Q. Zheng, R. T. Haasch, D. G. Sangiovanni, L. F. J. Piper, D. G. Schlom, Adsorption-controlled growth and properties of epitaxial SnO films. *Phys. Rev. Mater.* **3**, 105202 (2019).
75. C. D. Theis, J. Yeh, D. G. Schlom, M. E. Hawley, G. W. Brown, Adsorption-controlled growth of PbTiO₃ by reactive molecular beam epitaxy. *Thin Solid Films* **325**, 107–114 (1998).
76. B. Jalan, P. Moetakef, S. Stemmer, Molecular beam epitaxy of SrTiO₃ with a growth window. *Appl. Phys. Lett.* **95**, 032906 (2009).
77. D. G. Schlom, J. H. Haeni, J. Lettieri, C. D. Theis, W. Tian, J. C. Jiang, X. Q. Pan, Oxide nano-engineering using MBE. *Mater. Sci. Eng. B* **87**, 282–291 (2001).
78. J. Lapano, M. Brahlek, L. Zhang, J. Roth, A. Pogrebnikov, R. Engel-Herbert, Scaling growth rates for perovskite oxide virtual substrates on silicon. *Nat. Commun.* **10**, 2464 (2019).
79. H. Yoon, T. K. Truttman, F. Liu, B. E. Matthews, S. Choo, Q. Su, V. Saraswat, S. Manzo, M. S. Arnold, M. E. Bowden, J. K. Kawasaki, S. J. Koester, S. R. Spurgeon, S. A. Chambers, B. Jalan, Freestanding epitaxial SrTiO₃ nanomembranes via remote epitaxy using hybrid molecular beam epitaxy. *Sci. Adv.* **8**, eadd5328 (2022).
80. J. Son, P. Moetakef, B. Jalan, O. Bierwagen, N. J. Wright, R. Engel-Herbert, S. Stemmer, Epitaxial SrTiO₃ films with electron mobilities exceeding 30,000 cm²V⁻¹s⁻¹. *Nat. Mater.* **9**, 482–484 (2010).
81. A. Spinelli, M. A. Torija, C. Liu, C. Jan, C. Leighton, Electronic transport in doped SrTiO₃: Conduction mechanisms and potential applications. *Phys. Rev. B* **81**, 155110 (2010).
82. B. Jalan, S. J. Allen, G. E. Beltz, P. Moetakef, S. Stemmer, Enhancing the electron mobility of SrTiO₃ with strain. *Appl. Phys. Lett.* **98**, 132102 (2011).
83. Z. Yang, D. Lee, J. Yue, J. Gabel, T.-L. Lee, R. D. James, S. A. Chambers, B. Jalan, Epitaxial SrTiO₃ films with dielectric constants exceeding 25,000. *Proc. Natl. Acad. Sci. U.S.A.* **119**, e2202189119 (2022).
84. W. Nunn, S. Sandlass, M. Wegner, R. Haislmaier, A. Kumar, M. Tangi, J. LeBeau, E. Quandt, R. D. James, B. Jalan, Hybrid molecular beam epitaxy growth of BaTiO₃ films. *J. Vac. Sci. Technol. A* **39**, 040404 (2021).
85. Y. Matsubara, K. S. Takahashi, Y. Tokura, M. Kawasaki, Single-crystalline BaTiO₃ films grown by gas-source molecular beam epitaxy. *Appl. Phys. Express* **7**, 125502 (2014).
86. R. C. Haislmaier, E. D. Grimley, M. D. Biegalski, J. M. LeBeau, S. Trolier-McKinstry, V. Gopalan, R. Engel-Herbert, Unleashing strain induced ferroelectricity in complex oxide thin films via precise stoichiometry control. *Adv. Funct. Mater.* **26**, 7271–7279 (2016).
87. P. Moetakef, J. Y. Zhang, S. Raghavan, A. P. Kajdos, S. Stemmer, Growth window and effect of substrate symmetry in hybrid molecular beam epitaxy of a Mott insulating rare earth titanate. *J. Vac. Sci. Technol. A* **31**, 041503 (2013).
88. A. Prakash, P. Xu, X. Wu, G. Haugstad, X. Wang, B. Jalan, Adsorption-controlled growth and the influence of stoichiometry on electronic transport in hybrid molecular beam epitaxy-grown BaSnO₃ films. *J. Mater. Chem. C* **5**, 5730–5736 (2017).
89. T. Wang, L. R. Thoutam, A. Prakash, W. Nunn, G. Haugstad, B. Jalan, Defect-driven localization crossovers in MBE-grown La-doped SrSnO₃ films. *Phys. Rev. Mater.* **1**, 061601 (2017).
90. F. Liu, P. Golani, T. K. Truttman, I. Evangelista, M. A. Smeaton, D. Bugallo, J. Wen, A. K. Manjeshwar, S. J. May, L. F. Kourkoutis, A. Janotti, S. J. Koester, B. Jalan, Doping the undopable: Hybrid molecular beam epitaxy growth, n-Type doping, and field-effect transistor using CaSnO₃. *ACS Nano* **17**, 16912–16922 (2023).
91. H.-T. Zhang, L. R. Dedon, L. W. Martin, R. Engel-Herbert, Self-regulated growth of LaVO₃ thin films by hybrid molecular beam epitaxy. *Appl. Phys. Lett.* **106**, 233102 (2015).
92. M. Brahlek, L. Zhang, H.-T. Zhang, J. Lapano, L. R. Dedon, L. W. Martin, R. Engel-Herbert, Mapping growth windows in quaternary perovskite oxide systems by hybrid molecular beam epitaxy. *Appl. Phys. Lett.* **109**, 101903 (2016).
93. W. Nunn, A. Kumar, R. Zu, B. Nebgen, S. Yu, A. Kamath Manjeshwar, V. Gopalan, J. M. LeBeau, R. D. James, B. Jalan, Sn-modified BaTiO₃ thin film with enhanced polarization. *J. Vac. Sci. Technol. A* **41**, 022701 (2023).
94. F. Liu, T. K. Truttman, D. Lee, B. E. Matthews, I. Lارايب, A. Janotti, S. R. Spurgeon, S. A. Chambers, B. Jalan, Hybrid molecular beam epitaxy of germanium-based oxides. *Commun. Mater.* **3**, 69 (2022).
95. M. Brahlek, L. Zhang, C. Eaton, H.-T. Zhang, R. Engel-Herbert, Accessing a growth window for SrVO₃ thin films. *Appl. Phys. Lett.* **107**, 143108 (2015).
96. S. Thapa, S. R. Provence, P. T. Gemperline, B. E. Matthews, S. R. Spurgeon, S. L. Battles, S. M. Heald, M. A. Kuroda, R. B. Comes, Surface stability of SrNbO_{3+δ} grown by hybrid molecular beam epitaxy. *APL Mater.* **10**, 091112 (2022).
97. W. Nunn, A. K. Manjeshwar, J. Yue, A. Rajapitamahuni, T. K. Truttman, B. Jalan, Novel synthesis approach for “stubborn” metals and metal oxides. *Proc. Natl. Acad. Sci. U.S.A.* **118**, e2105713118 (2021).
98. S. Nair, Z. Yang, D. Lee, S. Guo, J. T. Sadowski, S. Johnson, A. Saboor, Y. Li, H. Zhou, R. B. Comes, W. Jin, K. A. Mkhoyan, A. Janotti, B. Jalan, Engineering metal oxidation using epitaxial strain. *Nat. Nanotechnol.* **18**, 1005–1011 (2023).

99. W. Nunn, S. Nair, H. Yun, A. Kamath Manjeshwar, A. Rajapitamahuni, D. Lee, K. A. Mkhoyan, B. Jalan, Solid-source metal-organic molecular beam epitaxy of epitaxial RuO_2 . *APL Mater.* **9**, 091112 (2021).
100. R. Choudhary, S. Nair, Z. Yang, D. Lee, B. Jalan, Semi-metallic SrIrO_3 films using solid-source metal-organic molecular beam epitaxy. *APL Mater.* **10**, 091118 (2022).
101. A. K. Manjeshwar, S. Nair, A. K. Rajapitamahuni, R. D. James, B. Jalan, Adsorption-controlled growth and magnetism in epitaxial SrRuO_3 films. *ACS Nano* **17**, 20999–21005 (2023).
102. R. Choudhary, Z. Liu, J. Cai, X. Xu, J.-H. Chu, B. Jalan, Growing clean crystals from dirty precursors: Solid-source metal-organic molecular beam epitaxy growth of superconducting Sr_2RuO_4 films. *APL Mater.* **11**, 061124 (2023).
103. S. Nair, K. Noordhoek, D. Lee, C. J. Bartel, B. Jalan, Solid-source metal-organic MBE for elemental Ir and Ru films. *J. Vac. Sci. Technol. A* **41**, 062701 (2023).
104. J. Kim, M. Yu, J.-W. Lee, S.-L. Shang, G.-Y. Kim, P. Pal, J. Seo, N. Campbell, K. Eom, R. Ramachandran, M. S. Rzchowski, S. H. Oh, S.-Y. Choi, Z.-K. Liu, J. Levy, C.-B. Eom, Electronic-grade epitaxial (111) KTaO_3 heterostructures. *Sci. Adv.* **10**, eadk4288 (2024).
105. L. P. Lee, M. J. Burns, K. Char, Free-standing microstructures of $\text{YBa}_2\text{Cu}_3\text{O}_{7-x}$: A high-temperature superconducting air bridge. *Appl. Phys. Lett.* **61**, 2706–2708 (1992).
106. J.-H. Kim, A. M. Grishin, Free-standing epitaxial $\text{La}_{1-x}(\text{Sr,Ca})_x\text{MnO}_3$ membrane on Si for uncooled infrared microbolometer. *Appl. Phys. Lett.* **87**, 033502 (2005).
107. S. G. Deutscher, E. Grunbaum, Method of producing monocrystalline semiconductor films utilizing an intermediate water dissolvable salt layer. US Patent 4,255,208 (1981).
108. M. Konagai, M. Sugimoto, K. Takahashi, High efficiency GaAs thin film solar cells by peeled film technology. *J. Cryst. Growth* **45**, 277–280 (1978).
109. D. Lu, D. J. Baek, S. S. Hong, L. F. Kourkoutis, Y. Hikita, H. Y. Hwang, Synthesis of freestanding single-crystal perovskite films and heterostructures by etching of sacrificial water-soluble layers. *Nat. Mater.* **15**, 1255–1260 (2016).
110. S. Varshney, S. Choo, L. Thompson, Z. Yang, J. Shah, J. Wen, S. J. Koester, K. A. Mkhoyan, A. S. McLeod, B. Jalan, Hybrid molecular beam epitaxy for single-crystalline oxide membranes with binary oxide sacrificial layers. *ACS Nano* **18**, 6348–6358 (2024).
111. S. S. Hong, M. Gu, M. Verma, V. Harbola, B. Y. Wang, D. Lu, A. Vaillonis, Y. Hikita, R. Pentcheva, J. M. Rondinelli, H. Y. Hwang, Extreme tensile strain states in $\text{La}_{0.7}\text{Ca}_{0.3}\text{MnO}_3$ membranes. *Science* **368**, 71–76 (2020).
112. P. Salles, I. Caño, R. Guzman, C. Dore, A. Mihi, W. Zhou, M. Coll, Facile chemical route to prepare water soluble epitaxial $\text{Sr}_3\text{Al}_2\text{O}_6$ sacrificial layers for free-standing oxides. *Adv. Mater. Interfaces* **8**, 2001643 (2021).
113. P. Salles, R. Guzman, A. Barrera, M. Ramis, J. M. Caicedo, A. Palau, W. Zhou, M. Coll, On the role of the $\text{Sr}_{1-x}\text{Ca}_x\text{Al}_2\text{O}_6$ sacrificial layer composition in epitaxial $\text{La}_{0.7}\text{Sr}_{0.3}\text{MnO}_3$ membranes. *Adv. Funct. Mater.* **33**, 2304059 (2023).
114. L. Nian, H. Sun, Z. Wang, D. Xu, B. Hao, S. Yan, Y. Li, J. Zhou, Y. Deng, Y. Hao, Y. Nie, $\text{Sr}_4\text{Al}_2\text{O}_7$: A new sacrificial layer with high water dissolution rate for the synthesis of freestanding oxide membranes. *Adv. Mater.* **36**, e2307682 (2024).
115. J. Zhang, T. Lin, A. Wang, X. Wang, Q. He, H. Ye, J. Lu, Q. Wang, Z. Liang, F. Jin, S. Chen, M. Fan, E.-J. Guo, Q. Zhang, L. Gu, Z. Luo, L. Si, W. Lu, L. Wang, Super-tetragonal $\text{Sr}_4\text{Al}_2\text{O}_7$ as a sacrificial layer for high-integrity freestanding oxide membranes. *Science* **383**, 388–394 (2024).
116. D. Pesquera, E. Khestanova, M. Ghidini, S. Zhang, A. P. Rooney, F. Maccherozzi, P. Riego, S. Farokhipoor, J. Kim, X. Moya, M. E. Vickers, N. A. Stelmashenko, S. J. Haigh, S. S. Dheshi, N. D. Mathur, Large magnetoelectric coupling in multiferroic oxide heterostructures assembled via epitaxial lift-off. *Nat. Commun.* **11**, 3190 (2020).
117. Y. Bourlier, B. Bérimi, M. Frégnaux, A. Fouchet, D. Aureau, Y. Dumont, Transfer of epitaxial SrTiO_3 nanothick layers using water-soluble sacrificial perovskite oxides. *ACS Appl. Mater. Interfaces* **12**, 8466–8474 (2020).
118. H. Peng, N. Lu, S. Yang, Y. Lyu, Z. Liu, Y. Bu, S. Shen, M. Li, Z. Li, L. Gao, S. Lu, M. Wang, H. Cao, H. Zhou, P. Gao, H. Chen, P. Yu, A generic sacrificial layer for wide-range freestanding oxides with modulated magnetic anisotropy. *Adv. Funct. Mater.* **32**, 2111907 (2022).
119. S. S. Hong, J. H. Yu, D. Lu, A. F. Marshall, Y. Hikita, Y. Cui, H. Y. Hwang, Two-dimensional limit of crystalline order in perovskite membrane films. *Sci. Adv.* **3**, eaao5173 (2017).
120. D. Ji, S. Cai, T. R. Paudel, H. Sun, C. Zhang, L. Han, Y. Wei, Y. Zang, M. Gu, Y. Zhang, W. Gao, H. Huyan, W. Guo, D. Wu, Z. Gu, E. Y. Tsybal, P. Wang, Y. Nie, X. Pan, Freestanding crystalline oxide perovskites down to the monolayer limit. *Nature* **570**, 87–90 (2019).
121. Q. Wang, H. Fang, D. Wang, J. Wang, N. Zhang, B. He, W. Lü, Towards a large-area freestanding single-crystal ferroelectric BaTiO_3 membrane. *Crystals* **10**, 733 (2020).
122. R. Qiu, B. Peng, H. Liu, Y. Guo, H. Tang, Z. Zhou, M. Liu, Epitaxial growth of pure $\text{Sr}_3\text{Al}_2\text{O}_6$ sacrificial layer for high quality freestanding single-crystalline oxide membranes. *Thin Solid Films* **773**, 139820 (2023).
123. P. T. P. Le, J. E. Ten Elshof, G. Koster, Epitaxial lift-off of freestanding (011) and (111) SrRuO_3 thin films using a water sacrificial layer. *Sci. Rep.* **11**, 12435 (2021).
124. Y. Li, E. Zatterin, M. Conroy, A. Pylpypets, F. Borodavka, A. Björling, D. J. Groenendijk, E. Lesne, A. J. Clancy, M. Hadjimichael, D. Kepaptsoglou, Q. M. Ramasse, A. D. Caviglia, J. Hlinka, U. Bangert, S. J. Leake, P. Zubko, Electrostatically driven polarization flow and strain-induced curvature in free-standing ferroelectric superlattices. *Adv. Mater.* **34**, e2106826 (2022).
125. D. Li, C. Adamo, B. Y. Wang, H. Yoon, Z. Chen, S. S. Hong, D. Lu, Y. Cui, Y. Hikita, H. Y. Hwang, Stabilization of $\text{Sr}_3\text{Al}_2\text{O}_6$ growth templates for ex situ synthesis of freestanding crystalline oxide membranes. *Nano Lett.* **21**, 4454–4460 (2021).
126. S. Cai, Y. Lun, D. Ji, P. Lv, L. Han, C. Guo, Y. Zang, S. Gao, Y. Wei, M. Gu, C. Zhang, Z. Gu, X. Wang, C. Addiego, D. Fang, Y. Nie, J. Hong, P. Wang, X. Pan, Enhanced polarization and abnormal flexural deformation in bent freestanding perovskite oxides. *Nat. Commun.* **13**, 5116 (2022).
127. H. Sun, J. Wang, Y. Wang, C. Guo, J. Gu, W. Mao, J. Yang, Y. Liu, T. Zhang, T. Gao, H. Fu, T. Zhang, Y. Hao, Z. Gu, P. Wang, H. Huang, Y. Nie, Nonvolatile ferroelectric domain wall memory integrated on silicon. *Nat. Commun.* **13**, 4332 (2022).
128. L. Han, X. Yang, Y. Lun, Y. Guan, F. Huang, S. Wang, J. Yang, C. Gu, Z.-B. Gu, L. Liu, Y. Wang, P. Wang, J. Hong, X. Pan, Y. Nie, Tuning piezoelectricity via thermal annealing at a freestanding ferroelectric membrane. *Nano Lett.* **23**, 2808–2815 (2023).
129. R. Takahashi, M. Lippmaa, Sacrificial water-soluble BaO layer for fabricating free-standing piezoelectric membranes. *ACS Appl. Mater. Interfaces* **12**, 25042–25049 (2020).
130. W. Cho, K. Sung, K.-S. An, S. Sook Lee, T.-M. Chung, Y. Kim, Atomic layer deposition of Al_2O_3 thin films using dimethylaluminum isopropoxide and water. *J. Vac. Sci. Technol. A* **21**, 1366–1370 (2003).
131. T. D.-M. Elko-Hansen, J. G. Ekerdt, XPS investigation of the atomic layer deposition half reactions of Bis(*N*-tert-butyl-*N'*-ethylpropionamidinato) cobalt(II). *Chem. Mater.* **26**, 2642–2646 (2014).
132. T. D.-M. Elko-Hansen, A. Dolocan, J. G. Ekerdt, Atomic interdiffusion and diffusive stabilization of cobalt by copper during atomic layer deposition from Bis(*N*-tert-butyl-*N'*-ethylpropionamidinato) cobalt(II). *J. Phys. Chem. Lett.* **5**, 1091–1095 (2014).
133. H. Shimizu, K. Shima, Y. Suzuki, T. Momose, Y. Shimogaki, Precursor-based designs of nano-structures and their processing for Co(W) alloy films as a single layered barrier/liner layer in future Cu-interconnect. *J. Mater. Chem. C* **3**, 2500–2510 (2015).
134. H. Li, Y. Gao, Y. Shao, Y. Su, X. Wang, Vapor-phase atomic layer deposition of Co_3S_2 and its application for supercapacitors. *Nano Lett.* **15**, 6689–6695 (2015).
135. A. W. Peters, Z. Li, O. K. Farha, J. T. Hupp, Atomically precise growth of catalytically active cobalt sulfide on flat surfaces and within a metal-organic framework via Atomic layer deposition. *ACS Nano* **9**, 8484–8490 (2015).
136. A. Devi, J. Goswami, R. Lakshmi, S. A. Shivashankar, S. Chandrasekaran, A novel Cu(II) chemical vapor deposition precursor: Synthesis, characterization, and chemical vapor deposition. *J. Mater. Res.* **13**, 687–692 (1998).
137. S. Varshney, M. Ramis, S. Choo, M. Coll, B. Jalan, Epitaxially grown single-crystalline SrTiO_3 membranes using a solution-processed, amorphous $\text{SrCa}_2\text{Al}_2\text{O}_6$ sacrificial layer. *J. Mater. Chem. C* **12**, 13809–13815 (2024).
138. A. J. Yang, S.-X. Wang, J. Xu, X. J. Loh, Q. Zhu, X. R. Wang, Two-dimensional layered materials meet perovskite oxides: A combination for high-performance electronic devices. *ACS Nano* **17**, 9748–9762 (2023).
139. Y.-H. Chu, Van der Waals oxide heteroepitaxy. *npj Quant. Mater.* **2**, 67 (2017).
140. Y. Kim, J. Watt, X. Ma, T. Ahmed, S. Kim, K. Kang, T. S. Luk, Y. J. Hong, J. Yoo, Fabrication of a microcavity prepared by remote epitaxy over monolayer molybdenum disulfide. *ACS Nano* **16**, 2399–2406 (2022).
141. D. Wang, Y. Lu, J. Meng, X. Zhang, Z. Yin, M. Gao, Y. Wang, L. Cheng, J. You, J. Zhang, Remote heteroepitaxy of atomic layered hafnium disulfide on sapphire through hexagonal boron nitride. *Nanoscale* **11**, 9310–9318 (2019).
142. W. Kong, H. Li, K. Qiao, Y. Kim, K. Lee, Y. Nie, D. Lee, T. Osadchy, R. J. Molnar, D. K. Gaskill, R. L. Myers-Ward, K. M. Daniels, Y. Zhang, S. Sundram, Y. Yu, S. Bae, S. Rajan, Y. Shao-Horn, K. Cho, A. Ougazzaden, J. C. Grossman, J. Kim, Polarity governs atomic interaction through two-dimensional materials. *Nat. Mater.* **17**, 999–1004 (2018).
143. H. Kim, K. Lu, Y. Liu, H. S. Kum, K. S. Kim, K. Qiao, S.-H. Bae, S. Lee, Y. J. Ji, K. H. Kim, H. Paik, S. Xie, H. Shin, C. Choi, J. H. Lee, C. Dong, J. A. Robinson, J.-H. Lee, J.-H. Ahn, G. Y. Yeom, D. G. Schlom, J. Kim, Impact of 2D–3D Heterointerface on remote epitaxial interaction through graphene. *ACS Nano* **15**, 10587–10596 (2021).
144. H. Kim, J. C. Kim, Y. Jeong, J. Yu, K. Lu, D. Lee, N. Kim, H. Y. Jeong, J. Kim, S. Kim, Role of transferred graphene on atomic interaction of GaAs for remote epitaxy. *J. Appl. Phys.* **130**, 174901 (2021).
145. X. Li, W. Cai, J. An, S. Kim, J. Nah, D. Yang, R. Piner, A. Velamakanni, I. Jung, E. Tutuc, S. K. Banerjee, L. Colombo, R. S. Ruoff, Large-area synthesis of high-quality and uniform graphene films on copper foils. *Science* **324**, 1312–1314 (2009).
146. B. Zhang, W. H. Lee, R. Piner, I. Kholmanov, Y. Wu, H. Li, H. Ji, R. S. Ruoff, Low-temperature chemical vapor deposition growth of graphene from toluene on electropolished copper foils. *ACS Nano* **6**, 2471–2476 (2012).
147. X. Li, Y. Zhu, W. Cai, M. Borysiak, B. Han, D. Chen, R. D. Piner, L. Colombo, R. S. Ruoff, Transfer of large-area graphene films for high-performance transparent conductive electrodes. *Nano Lett.* **9**, 4359–4363 (2009).
148. J. Kim, H. Park, J. B. Hannon, S. W. Bedell, K. Fogel, D. K. Sadana, C. Dimitrakopoulos, Layer-resolved graphene transfer via engineered strain layers. *Science* **342**, 833–836 (2013).
149. J. Sun, T. Gao, X. Song, Y. Zhao, Y. Lin, H. Wang, D. Ma, Y. Chen, W. Xiang, J. Wang, Y. Zhang, Z. Liu, Direct growth of high-quality graphene on high- κ dielectric SrTiO_3 substrates. *J. Am. Chem. Soc.* **136**, 6574–6577 (2014).

150. S. Karamat, K. Çelik, A. Oral, Growth of nano-graphene on SrTiO₃ (110) substrates by chemical vapour deposition. *Mater. Chem. Phys.* **200**, 187–195 (2017).
151. Z. Chen, C. Xie, W. Wang, J. Zhao, B. Liu, J. Shan, X. Wang, M. Hong, L. Lin, L. Huang, X. Lin, S. Yang, X. Gao, Y. Zhang, P. Gao, K. S. Novoselov, J. Sun, Z. Liu, Direct growth of wafer-scale highly oriented graphene on sapphire. *Sci. Adv.* **7**, eabk0115 (2021).
152. M. A. Fanton, J. A. Robinson, C. Puls, Y. Liu, M. J. Hollander, B. E. Weiland, M. LaBella, K. Trumbull, R. Kasarda, C. Howsare, J. Stitt, D. W. Snyder, Characterization of graphene films and transistors grown on sapphire by metal-free chemical vapor deposition. *ACS Nano* **5**, 8062–8069 (2011).
153. J. Shan, J. Sun, Z. Liu, Chemical vapor deposition synthesis of graphene over sapphire substrates. *ChemNanoMat* **7**, 515–525 (2021).
154. P. R. Kidambi, B. C. Bayer, R. S. Weatherup, R. Ochs, C. Ducati, D. V. Szabó, S. Hofmann, Hafnia nanoparticles—A model system for graphene growth on a dielectric. *Phys. Status Solidi Rapid Res. Lett.* **5**, 341–343 (2011).
155. J. Ji, S. Park, H. Do, H. S. Kum, A review on recent advances in fabricating freestanding single-crystalline complex-oxide membranes and its applications. *Phys. Scr.* **98**, 052002 (2023).
156. S. Han, Y. Meng, Z. Xu, J. S. Kim, Y. Li, I.-P. Roh, H. Ahn, D.-H. Kim, S.-H. Bae, Freestanding membranes for unique functionality in electronics. *ACS Appl. Electron. Mater.* **5**, 690–704 (2023).
157. X. Yan, H. Cao, Y. Li, H. Hong, D. J. Gosztola, N. P. Guisinger, H. Zhou, D. D. Fong, In situ x-ray studies of growth of complex oxides on graphene by molecular beam epitaxy. *APL Mater.* **10**, 091114 (2022).
158. D. Du, T. Jung, S. Manzo, Z. LaDuca, X. Zheng, K. Su, V. Saraswat, J. McChesney, M. S. Arnold, J. K. Kawasaki, Controlling the balance between remote, pinhole, and van der Waals epitaxy of heusler films on graphene/sapphire. *Nano Lett.* **22**, 8647–8653 (2022).
159. C. S. Chang, K. S. Kim, B.-I. Park, J. Choi, H. Kim, J. Jeong, M. Barone, N. Parker, S. Lee, X. Zhang, K. Lu, J. M. Suh, J. Kim, D. Lee, N. M. Han, M. Moon, Y. S. Lee, D.-H. Kim, D. G. Schlom, Y. J. Hong, J. Kim, Remote epitaxial interaction through graphene. *Sci. Adv.* **9**, eadj5379 (2023).
160. L. Dai, G. Niu, J. Zhao, H. Zhao, Y. Liu, Y. Wang, Y. Zhang, H. Wu, L. Wang, D. Pfützenreuter, J. Schwarzkopf, C. Dubourdieu, T. Schroeder, Z.-G. Ye, Y.-H. Xie, W. Ren, Toward van der Waals epitaxy of transferable ferroelectric barium titanate films via a graphene monolayer. *J. Mater. Chem. C* **8**, 3445–3451 (2020).
161. S.-H. Bae, K. Lu, Y. Han, S. Kim, K. Qiao, C. Choi, Y. Nie, H. Kim, H. S. Kum, P. Chen, W. Kong, B.-S. Kang, C. Kim, J. Lee, Y. Baek, J. Shim, J. Park, M. Joo, D. A. Muller, K. Lee, J. Kim, Graphene-assisted spontaneous relaxation towards dislocation-free heteroepitaxy. *Nat. Nanotechnol.* **15**, 272–276 (2020).
162. Y. Kim, S. S. Cruz, K. Lee, B. O. Alawode, C. Choi, Y. Song, J. M. Johnson, C. Heidelberger, W. Kong, S. Choi, K. Qiao, I. Almansouri, E. A. Fitzgerald, J. Kong, A. M. Kolpak, J. Hwang, J. Kim, Remote epitaxy through graphene enables two-dimensional material-based layer transfer. *Nature* **544**, 340–343 (2017).
163. J. Jiang, X. Sun, X. Chen, B. Wang, Z. Chen, Y. Hu, Y. Guo, L. Zhang, Y. Ma, L. Gao, F. Zheng, L. Jin, M. Chen, Z. Ma, Y. Zhou, N. P. Padture, K. Beach, H. Terrones, Y. Shi, D. Gall, T.-M. Lu, E. Wertz, J. Feng, J. Shi, Carrier lifetime enhancement in halide perovskite via remote epitaxy. *Nat. Commun.* **10**, 4145 (2019).
164. S. Manzo, K. Su, M. S. Arnold, J. K. Kawasaki, Nucleation selectivity and lateral coalescence of GaAs over graphene on Ge(111). *ACS Appl. Mater. Interfaces* **15**, 59905–59911 (2023).
165. Z. LaDuca, K. Su, S. Manzo, M. S. Arnold, J. K. Kawasaki, Control of ternary alloy composition during remote epitaxy on graphene. *Phys. Rev. Mater.* **7**, 083401 (2023).
166. Z. H. Lim, S. Manzo, P. J. Strohbeen, V. Saraswat, M. S. Arnold, J. K. Kawasaki, Selective area epitaxy of GaAs films using patterned graphene on Ge. *Appl. Phys. Lett.* **120**, 051603 (2022).
167. J. W. Hutchinson, Z. Suo, “Mixed mode cracking in layered materials” in *Advances in Applied Mechanics* (Elsevier, 1991), vol. 29, pp. 63–191.
168. F. Dross, J. Robbelein, B. Vandeveld, E. Van Kerschaver, I. Gordon, G. Beaucarne, J. Poortmans, Stress-induced large-area lift-off of crystalline Si films. *Appl. Phys. A* **89**, 149–152 (2007).
169. S. W. Bedell, P. Lauro, J. A. Ott, K. Fogel, D. K. Sadana, Layer transfer of bulk gallium nitride by controlled spalling. *J. Appl. Phys.* **122**, 025103 (2017).
170. A. Sambri, M. Scuderi, A. Guarino, E. D. Gennaro, R. Erlandsen, R. T. Dahm, A. V. Bjorlig, D. V. Christensen, R. D. Capua, B. D. Ventura, U. S. D. Uccio, S. Mirabella, G. Nicotra, C. Spinella, T. S. Jespersen, F. M. Granozio, Self-formed, conducting LaAlO₃/SrTiO₃ micro-membranes. *Adv. Funct. Mater.* **30**, 1909964 (2020).
171. R. T. Dahm, R. Erlandsen, F. Trier, A. Sambri, E. D. Gennaro, A. Guarino, L. Stampfer, D. V. Christensen, F. M. Granozio, T. S. Jespersen, Size-controlled spalling of LaAlO₃/SrTiO₃ micromembranes. *ACS Appl. Mater. Interfaces* **13**, 12341–12346 (2021).
172. R. Erlandsen, R. T. Dahm, F. Trier, M. Scuderi, E. Di Gennaro, A. Sambri, C. K. Reffeldt Kirchert, N. Pryds, F. M. Granozio, T. S. Jespersen, A two-dimensional superconducting electron gas in freestanding LaAlO₃/SrTiO₃ micro-membranes. *Nano Lett.* **22**, 4758–4764 (2022).
173. G. F. Schneider, V. E. Calado, H. Zandbergen, L. M. K. Vandersypen, C. Dekker, Wedging transfer of nanostructures. *Nano Lett.* **10**, 1912–1916 (2010).
174. K. J. Edgar, C. M. Buchanan, J. S. Debenham, P. A. Rundquist, B. D. Seiler, M. C. Shelton, D. Tindall, Advances in cellulose ester performance and application. *Prog. Polym. Sci.* **26**, 1605–1688 (2001).
175. Y. Cheng, Y. Li, G. Dong, B. Peng, Z. Zhou, M. Liu, Flexible multiferroic heterostructure based on freestanding single-crystalline BaTiO₃ membranes for spintronic devices. *Adv. Electron. Mater.* **8**, 2100923 (2022).
176. B. Zhang, C. Yun, J. L. MacManus-Driscoll, High yield transfer of clean large-area epitaxial oxide thin films. *Nanomicro Lett.* **13**, 39 (2021).
177. J. Shin, H. Kim, S. Sundaram, J. Jeong, B.-I. Park, C. S. Chang, J. Choi, T. Kim, M. Saravanapavantham, K. Lu, S. Kim, J. M. Suh, K. S. Kim, M.-K. Song, Y. Liu, K. Qiao, J. H. Kim, Y. Kim, J.-H. Kang, J. Kim, D. Lee, J. Lee, J. S. Kim, H. E. Lee, H. Yeon, H. S. Kum, S.-H. Bae, V. Bulovic, K. J. Yu, K. Lee, K. Chung, Y. J. Hong, A. Ougazzaden, J. Kim, Vertical full-colour micro-LEDs via 2D materials-based layer transfer. *Nature* **614**, 81–87 (2023).
178. H. Kim, S. Lee, J. Shin, M. Zhu, M. Akl, K. Lu, N. M. Han, Y. Baek, C. S. Chang, J. M. Suh, K. S. Kim, B.-I. Park, Y. Zhang, C. Choi, H. Shin, H. Yu, Y. Meng, S.-I. Kim, S. Seo, K. Lee, H. S. Kum, J.-H. Lee, J.-H. Ahn, S.-H. Bae, J. Hwang, Y. Shi, J. Kim, Graphene nanopattern as a universal epitaxy platform for single-crystal membrane production and defect reduction. *Nat. Nanotechnol.* **17**, 1054–1059 (2022).
179. K. Gu, T. Katayama, S. Yasui, A. Chikamatsu, S. Yasuhara, M. Itoh, T. Hasegawa, Simple method to obtain large-size single-crystalline oxide sheets. *Adv. Funct. Mater.* **30**, 2001236 (2020).
180. D. Kim, W. K. Jung, S. Lee, Single-crystalline-level properties of ultrathin SrRuO₃ flexible membranes with wide and clean surface. *npj Flex. Electron.* **6**, 24 (2022).
181. S. Yun, T. E. Le Cozannet, C. H. Christoffersen, E. Brand, T. S. Jespersen, N. Pryds, Strain engineering: Perfecting freestanding perovskite oxide fabrication. *Small* **20**, 2310782 (2024).
182. L. Gong, M. Wei, R. Yu, H. Ohta, T. Katayama, Significant suppression of cracks in freestanding perovskite oxide flexible sheets using a capping oxide layer. *ACS Nano* **16**, 21013–21019 (2022).
183. H. Guo, Z. Hu, Z. Liu, J. Tian, Stacking of 2D materials. *Adv. Funct. Mater.* **31**, 2007810 (2021).
184. Y. Chen, Y. Tang, F. Gong, B. Wu, M. Han, M. Zou, Y. Feng, Y. Wang, Y. Zhu, X. Ma, Direct observation of large-scale screw dislocation grids in oxide heteroepitaxies. *Nano Lett.* **22**, 2085–2093 (2022).
185. A. Bhattacharya, S. J. May, Magnetic oxide heterostructures. *Annu. Rev. Mater. Res.* **44**, 65–90 (2014).
186. H. Liu, R. D. James, Design of origami structures with curved tiles between the creases. *J. Mech. Phys. Solids* **185**, 105559 (2024).
187. G. Sánchez-Santolino, V. Rouco, S. Puebla, H. Aramberri, V. Zamora, M. Cabero, F. A. Cuellar, C. Munuera, F. Mompean, M. Garcia-Hernandez, A. Castellanos-Gomez, J. Íñiguez, C. Leon, J. Santamaría, A 2D ferroelectric vortex pattern in twisted BaTiO₃ freestanding layers. *Nature* **626**, 529–534 (2024).
188. J. Kim, M. You, K.-E. Kim, K. Chu, C.-H. Yang, Artificial creation and separation of a single vortex–antivortex pair in a ferroelectric flatland. *npj Quantum Mater.* **4**, 29 (2019).
189. D. Du, J. Hu, J. K. Kawasaki, Strain and strain gradient engineering in membranes of quantum materials. *Appl. Phys. Lett.* **122**, 170501 (2023).
190. D. G. Schlom, L.-Q. Chen, C.-B. Eom, K. M. Rabe, S. K. Streiffer, J.-M. Triscone, Strain tuning of ferroelectric thin films. *Annu. Rev. Mater. Res.* **37**, 589–626 (2007).
191. S. Pezzini, V. Mišeiškis, G. Piccinini, S. Forti, S. Pace, R. Engelke, F. Rossella, K. Watanabe, T. Taniguchi, P. Kim, C. Coletti, 30°-twisted bilayer graphene quasicrystals from chemical vapor deposition. *Nano Lett.* **20**, 3313–3319 (2020).

Acknowledgments

Funding: S.C. and B.J. acknowledge partial support from the Air Force Office of Scientific Research (AFOSR) through grant nos. FA9550-21-1-0025 and FA9550-21-0460. This work also benefitted from the Vannevar Bush Faculty Fellowship N00014-19-1-2623. R.D.J. also acknowledges support from the AFOSR through grant no. FA9550-23-1-0093. S.V. and B.J. acknowledge support from the U.S. Department of Energy through grant no. DE-SC0020211 and the Center for Programmable Energy Catalysis, an Energy Frontier Research Center funded by the U.S. Department of Energy, Office of Science, Basic Energy Sciences at the University of Minnesota, under award no. DE-SC0023464. **Author contributions:** S.V., S.C., and B.J. wrote the first draft of the manuscript. H.L., S.S., and R.D.J. provided additional text and edits. All authors approved the final draft. **Competing interests:** The authors declare that they have no competing interests. **Data and materials availability:** All data needed to evaluate the conclusions in the paper are present in the paper.

Submitted 3 June 2024

Accepted 4 November 2024

Published 11 December 2024

10.1126/sciadv.adq8561